JOURNAL OF VIROLOGY, May 2009, p. 4895–4911 Vol. 83, No. 10
0022-538X/09/$08.00+0 doi:10.1128/JVI.02498-08

Kaposi's Sarcoma-Associated Herpesvirus Utilizes an Actin Polymerization-Dependent Macropinocytic Pathway To Enter Human Dermal Microvascular Endothelial and Human Umbilical Vein Endothelial Cells[▽]

Hari Raghu, Neelam Sharma-Walia, Mohanan Valiya Veettil, Sathish Sadagopan, and Bala Chandran*

H. M. Bligh Cancer Research Laboratories, Department of Microbiology and Immunology, Chicago Medical School, Rosalind Franklin University of Medicine and Science, North Chicago, Illinois

Received 4 December 2008/Accepted 3 March 2009

Kaposi's sarcoma-associated herpesvirus (KSHV) utilizes clathrin-mediated endocytosis for its infectious entry into human foreskin fibroblast (HFF) cells (S. M. Akula, P. P. Naranatt, N.-S. Walia, F.-Z. Wang, B. Fegley, and B. Chandran, J. Virol. 77:7978–7990, 2003). Here, we characterized KSHV entry into primary human microvascular dermal endothelial (HMVEC-d) and human umbilical vein endothelial (HUVEC) cells. Similar to the results for HMVEC-d cells, KSHV infection of HUVEC cells also resulted in an initial high level and subsequent decline in the expression of the lytic switch gene, ORF50, while latent gene expression persisted. Internalized virus particles enclosed in irregular vesicles were observed by electron microscopy of infected HMVEC-d cells. At an early time of infection, colocalization of KSHV capsid with envelope was observed by immunofluorescence analysis, thus demonstrating endocytosis of intact enveloped virus particles. Chlorpromazine, an inhibitor of clathrin-mediated endocytosis, and filipin ($C_{35}H_{58}O_{11}$), a caveolar endocytosis inhibitor, did not have any effect on KSHV binding, entry (DNA internalization), or gene expression in HMVEC-d and HUVEC cells. In contrast to the results for HFF cells, virus entry and gene expression in both types of endothelial cells were significantly blocked by macropinocytosis inhibitors (EIPA [5-*N*-ethyl-*N*-isoproamiloride] and rottlerin [$C_{30}H_{28}O_8$]) and by cytochalasin D, which affects actin polymerization. Inhibition of lipid raft blocked viral gene expression in HMVEC-d cells but not in HUVEC or HFF cells. In HMVEC-d and HUVEC cells, KSHV induced the actin polymerization and formation of lamellipodial extensions that are essential for macropinocytosis. Inhibition of macropinocytosis resulted in the distribution of viral capsids at the HMVEC-d cell periphery, and capsids did not associate with microtubules involved in the nuclear delivery of viral DNA. Internalized KSHV in HMVEC-d and HUVEC cells colocalized with the macropinocytosis marker dextran and not with the clathrin pathway marker transferrin or with caveolin. Dynasore, an inhibitor of dynamin, did not block viral entry into endothelial cells but did inhibit entry into HFF cells. KSHV was not associated with the early endosome marker EEA-1 in HMVEC-d cells, but rather with the late endosome marker LAMP1, as well as with Rab34 GTPase that is known to regulate macropinocytosis. Silencing Rab34 with small interfering RNA dramatically inhibited KSHV gene expression. Bafilomycin-mediated disruption of endosomal acidification inhibited viral gene expression. Taken together, these findings suggest that KSHV utilizes the actin polymerization-dependent, dynamin-independent macropinocytic pathway that involves a Rab34 GTPase-dependent late endosome and low-pH environment for its infectious entry into HMVEC-d and HUVEC cells. These studies also demonstrate that KSHV utilizes different modes of endocytic entry in fibroblast and endothelial cells.

DNA of Kaposi's sarcoma-associated herpesvirus (KSHV), or human herpesvirus 8 (HHV-8), has been detected in KS tissues from patients with AIDS-KS, classic KS, African endemic KS, and transplantation-associated KS (6, 9, 12, 49, 50). Several follow-up studies strongly suggest an etiological association of KSHV in the pathogenesis of KS and with two B-lymphoproliferative diseases, namely, body cavity-based B cell lymphoma (BCBL), or primary effusion lymphoma, and multicentric Castleman's disease (6, 12, 49, 50). The in vivo host cell range of KSHV is not yet fully characterized but appears to be broad, in that viral DNA and transcripts have been detected in B cells from peripheral blood, B cells of BCBL and multicentric Castleman's disease, flat endothelial cells lining the vascular spaces of KS lesions, typical KS spindle cells, $CD45^+/CD68^+$ monocytes in KS lesions, keratinocytes, and epithelial cells (10, 12, 29). KSHV DNA is present in a latent form in the vascular endothelial and spindle cells of KS tissues, and the expression of latency-associated LANA-1 (open reading frame 73 [ORF73]), v-cyclin D (ORF72), v-FLIP (K13), and Kaposin (K12) genes has been demonstrated in these cells (10, 12, 50, 57, 68). Lytic infection is also detected in KS lesions with <1% of infiltrating inflammatory monocytic cells positive for lytic cycle proteins (10, 12).

In vitro, KSHV has been shown to infect a variety of human cells, such as B cells, endothelial cells, epithelial cells, and fibroblast cells (2, 4). In addition, KSHV also infects a variety

* Corresponding author. Mailing address: Department of Microbiology and Immunology, H. M. Bligh Cancer Research Laboratories, Chicago Medical School, Rosalind Franklin University of Medicine and Science, 3333 Green Bay Road, North Chicago, IL 60064. Phone: (847) 578-8822. Fax: (847) 578-3349. E-mail: bala.chandran@rosalindfranklin.edu.

▽ Published ahead of print on 11 March 2009.

of animal cells, such as owl monkey kidney cells, baby hamster kidney fibroblast cells, Chinese hamster ovary cells, and primary embryonic mouse fibroblast cells (3, 11, 31, 45, 50, 62). In contrast to alpha- and betaherpesviruses, in vitro infection by KSHV does not result in a productive lytic cycle. Instead, KSHV infection of human microvascular dermal endothelial (HMVEC-d) and human foreskin fibroblast (HFF) cells is characterized by the sustained expression of latency-associated genes (8, 9, 14, 21). A unique aspect of this in vitro infection is our demonstration of the concurrent expression of a limited set of lytic cycle genes with antiapoptotic and immune modulation functions, including the lytic cycle switch, or Rta, gene, ORF50 (21). While the expression of latent ORF72, ORF73, and K13 genes continues, that of nearly all lytic genes declines (8, 21). However, this in vitro latency is unstable, and the viral DNA is not maintained efficiently and is usually lost over time during subsequent culturing of the infected cells (8, 9, 14, 21).

The mode of KSHV entry into the different target cells is not fully explored. Our earlier studies have shown that KSHV utilizes clathrin-mediated endocytosis and a low-pH environment for its infectious entry into HFF cells. Electron-microscopic observation of infected BJAB (KSHV- and Epstein-Barr virus-negative B lymphoma) cells demonstrated virus entry via large uncharacterized vesicles (4). Studies using agents blocking the acidification of endosomes suggested a low-pH-dependent endocytic infectious entry pathway in HEK 293 cells (human embryonic kidney epithelial cells). A recent study also suggested endocytosis as the mode of KSHV entry into activated primary human B cells (44). However, the nature of endocytic vesicles in B, epithelial (HEK 293), and endothelial cells is unknown.

Here, we examined the mode of entry into two types of human endothelial cells, HMVEC-d cells and umbilical vein endothelial (HUVEC) cells. Our studies demonstrate that, in contrast to HFF cells, KSHV utilizes the macropinocytic pathway as one of the major pathways for its infectious entry.

MATERIALS AND METHODS

Cells and viruses. HMVEC-d cells and HUVEC cells were grown in EBM-2 medium (CC-2543; Lonza biosciences, Basel, Switzerland), and HFF cells (Clonetics, Walkersville, MD) were grown in Dulbecco's modified Eagle's medium (Gibco BRL, Grand Island, NY) supplemented with 10% heat-inactivated fetal bovine serum (HyClone, Logan, UT). BCBL-1 cells (KSHV-carrying human B cells) used in the present study were propagated and maintained as described previously (30–32, 43, 47, 51, 55, 60, 64). Induction of the lytic cycle of KSHV from BCBL-1 cells, collection of virus from the supernatant, and viral purification were carried out as described previously (30–32, 43, 47, 51, 55, 60, 64). Virus purity was assessed according to general guidelines established in our laboratory. KSHV DNA was extracted from the virus, and copy numbers were quantitated by real-time DNA PCR using primers amplifying the KSHV ORF73 gene as described previously (3, 21, 31).

Antibodies and reagents. MβCD, nystatin, heparin, LY294002 [20(4-morphodionyl)-8-phenyl-1(4H)-benzopyran-4-one], cytochalasin D, chlorpromazine, EIPA (5-*N*-ethyl-*N*-isoproamiloride), rottlerin ($C_{30}H_{28}O_8$), filipin, bafilomycin A1, NH_4Cl, dynasore, tetradeconyl-phorbol acetate, lysophosphatidic acid, cholera toxin B, Triton X-100, and antibodies to tubulin were obtained from Sigma, St. Louis, MO. Monoclonal antibody (mAb) to EEA-1 (early endosomal antigen 1) was obtained from BD biosciences, San Jose, CA. Antibody to LAMP-1 was obtained from the Iowa Hybridoma Bank, Iowa. Antibodies to Rab5 were obtained from Abcam, Cambridge, MA. Antibodies for Rab34 and anti-human transferrin were obtained from Santa Cruz Biotechnology, Inc., Santa Cruz, CA. Anti-rabbit, anti-goat, and anti-mouse secondary antibodies linked to Alexa Fluor 488 and 594 and Alexa Fluor 488-labeled phalloidin and dextran TR (molecular weight, 70,000) were obtained from Molecular Probes, Eugene, OR.

Radiolabeled-KSHV binding assay. HMVEC-d cells were preincubated with nontoxic doses of various inhibitors before the addition of [^{3}H]thymidine-labeled, density gradient-purified KSHV (5,000 cpm) (43). As a control, labeled KSHV was incubated with 100 μg of heparin/ml for 90 min at 4°C, added to HMVEC-d cells, and incubated for 90 min at 4°C. After incubation, the cells were washed five times and lysed with 1% sodium dodecyl sulfate and 1% Triton X-100, and the radioactive virus was precipitated with trichloroacetic acid and counted in a scintillation counter.

Cytotoxicity assays. Target cells were incubated with medium containing different concentrations of various inhibitors for 4 h. Supernatants were collected and assessed for cellular toxicity by using a lactate dehydrogenase cytotoxicity assay kit (Promega, Madison, WI) in accordance with the manufacturer's recommendations.

Preparation of DNA and RNA. Isolation of total DNAs from the viral stocks and HMVEC-d cells by using a DNeasy tissue kit (Qiagen, Inc., Valencia, CA) and isolation of total RNA from infected or uninfected cells by using an RNeasy kit were carried out as described previously (21).

Measurement of KSHV DNA internalization by real-time DNA PCR. HMVEC-d cells that were left untreated or incubated with nontoxic concentrations of different inhibitors for 1 h at 37°C were infected with KSHV at a multiplicity of infection (MOI) of 10. At different time points of incubation with virus, cells were washed twice with Hanks' balanced salt solution (HBSS) to remove unbound virus. Cells were treated with 0.25% trypsin–EDTA for 5 min at 37°C to remove the bound noninternalized virus. Detached cells were washed twice to remove the virus and trypsin-EDTA. Total DNA isolated from cells was tested by real-time PCR for ORF73 as described previously (21).

Real-time RT-PCR. For RNA isolation, infected cells were lysed at different time points using lysis buffer provided in the RNeasy kit, with DNase I digestion (Qiagen, Valencia, CA). Two micrograms of total RNA was converted to cDNA with ThermoScript reverse transcriptase, using random hexamers (Invitrogen, Carlsbad, CA). The relative abundance of target gene mRNA, as well as the internal control cyclophilin A or hypoxanthine phosphoribosyltransferase (HPRT), was measured by real-time inverse transcription PCR (RT-PCR). The ORF50 and ORF73 transcripts were detected by real-time RT-PCR using gene-specific real-time primers and specific TaqMan probes as described previously (21, 55). The primers used for the other genes are as follows: K8 forward, 5′-CTGGACGCTCTCTCACACA-3′; K8 reverse, 5′-GATCTGCGAGTTGGAAGCT-3′; gpK8.1 forward, 5′-AATATCAGCCTTTTCAGGATCA-3′; gpK8.1 reverse, 5′-CACCACTATTTCTGCCGTTTTC-3′; HPRT forward, 5′-GGACAGGACTGAACGTCTTGC-3′; HPRT reverse, 5′-CTTGAGCACACAGAGGGCTACA-3′; cyclophilin A forward, 5′-GTCGACGGCGAGCCC-3′; cyclophilin A reverse, 5′-TCTTTGGGACCTTGTCTGCAA-3′; glyceraldehyde-3-phosphate dehydrogenase (GAPDH) forward, 5′-ATTCCATGGCACCGTCAAGGCT-3′; and GAPDH reverse, 5′-TCAGGTCCACCACTGACACGT-3′. The standard amplification program included 40 cycles of two steps each comprised of heating to 95°C and 60°C. The fluorescent product was detected at the last step of each cycle. Relative quantification of PCR products was calculated after normalization to the level of the endogenous control using cyclophilin A or HPRT (55).

Plasmid transfections. Transfection of HMVEC-d cells with wild-type (WT) dynamin (1 μg) or K44A (1 μg) plasmids was performed by using Effectene transfection reagent (Qiagen) according to the manufacturer's instructions. The transfection efficiencies with plasmids, as determined by green fluorescent protein (GFP) expression, were 30 to 40%.

Immunofluorescence microscopy. HMVEC-d or HUVEC cells grown in eight-chamber slides were infected or left uninfected for different times and stained for primary antibody to EEA-1, LAMP 1, phalloidin-Alexa Fluor 488, Rab5, and Rab34 antibodies, as well as antibodies against viral glycoprotein gpK8.1A and ORF65 capsid protein, wherever applicable and then stained with anti-mouse or anti-rabbit antibodies against endocytic markers and viral markers.

For transferrin and dextran colocalization with virus, cells were incubated with Texas Red-labeled dextran (0.5 mg/ml) and KSHV at an MOI of 10 or with 35 μg/ml of Alexa Fluor 594-conjugated transferrin and KSHV at an MOI of 10 for 5, 10, and 15 min at 37°C. The cells were washed in HBSS, fixed in 2% paraformaldehyde for 15 min, permeabilized with 0.2% Triton X-100 for 5 min, and blocked with 5% bovine serum albumin (BSA) for 15 min. Cells were incubated with anti-gpK8.1A mAb at room temperature for 1 h and stained with Alexa Fluor 488-conjugated goat anti-mouse secondary antibodies at room temperature for 1 h. For colocalization studies with virus and caveolin, cells were incubated with KSHV at an MOI of 10 for 5, 10, and 15 min at 37°C, followed by fixation with 4% paraformaldehyde for 15 min, and permeabilized with 0.2% Triton X-100 for 5 min at room temperature. After being blocked for 15 min with 10% BSA, cells were processed for double immunostaining with antibodies

against gpK8.1A and caveolin. This was followed by 1 h of incubation at room temperature with goat anti-mouse antibody labeled with Alexa Fluor 488 and goat anti-rabbit antibody labeled with Alexa Fluor 594. Following washing with phosphate-buffered saline (PBS), slides were mounted with mounting medium containing 4′,6′-diamidino-2-phenylindole (DAPI) and examined under a Nikon fluorescent microscope equipped with a Metamorph digital imaging system.

Laser-scanning confocal immunofluorescence microscopy. HMVEC-d cells infected with KSHV at an MOI of 10 were fixed with 4% paraformaldehyde. Cells were then permeabilized with 0.2% Triton X-100 for 5 min, washed, and blocked with goat serum for 30 min. The samples were then incubated for 1 h with primary antibody to gpK8.1A, Rab5, or Rab34 for 1 h at room temperature. The cells were then stained with appropriate secondary antibody linked with Alexa Fluor 488 or Alexa Fluor 594. An Olympus Fluoview 300 fluorescent confocal microscope was used for imaging, and analysis was performed using Fluoview software (Olympus, Melville, NY).

Electron microscopy. HMVEC-d cells grown in 75-cm^2 flasks were left untreated and washed three or four times with PBS. The cells were infected with KSHV at an MOI of 20 at 4°C for 1 h, and then the temperature was shifted to 37°C and infection was done for 5 and 10 min. After each time point, cells were washed and pelleted. The cells were fixed in 2% glutaraldehyde, rinsed in PBS, postfixed in 1% osmium tetroxide, dehydrated in a graded ethanol series, and embedded in 812 resin. Thin sections were made and visualized under a JEOL 100CXII transmission electron microscope.

Rab34 silencing. Rab34 silencing was done by using Rab34 small interfering RNA (siRNA) according to the manufacturer's protocol (Santa Cruz Biotechnology). Briefly, 2×10^5 HMVEC-d cells were transfected in a six-well tissue culture plate in 2 ml of antibiotic-free normal growth medium supplemented with fetal bovine serum. A low passage number (six) of HMVEC-d cell cultures was used for all transfection studies, and the viability of transfected cells was checked. Transfected cells were kept at 37°C for 24 h and 48 h in a CO_2 incubator. RNA was isolated from si-control (si-C)- or si-Rab34-transfected HMVEC-d cells and converted to cDNA, and the expression of Rab34 was measured by quantitative RT-PCR using Rab34-specific primers. Relative quantification of the PCR product for Rab34 was calculated after normalization to the level of endogenous control GAPDH. Rab34 silencing was calculated by considering the level of Rab34 in the untransfected cells or the si-C-transfected cells to be 100%. At 24 h posttransfection with si-C or si-Rab34, HMVEC-d cells were infected for 2, 8, and 24 h with KSHV at an MOI of 10; total RNA was collected, and ORF50 and ORF73 transcripts were detected by quantitative RT-PCR using gene-specific real-time primers and specific TaqMan probes (Applied Biosystems, Foster City, CA).

RESULTS

KSHV enters HMVEC-d cells by endocytosis. Studies by us and others have shown that KSHV utilizes endocytosis as a mode of entry to infect HFF, BJAB, HEK 293, and activated primary human B cells (1, 4). When KSHV-infected HMVEC-d cells at 5 min postinfection (p.i.) were examined by transmission electron microscopy, internalized enveloped viral particles in large, irregular-shaped endocytic vesicles were observed (Fig. 1A, a to c). In repeated examinations of different samples, we did not observe fusion of virion envelope with the plasma membranes of HMVEC-d cells. However, we did observe the fusion of virion envelope with endocytic vesicle membranes of HMVEC-d cells (Fig. 1A, d). These observations indicate that KSHV enters HMVEC-d cells by endocytosis.

To confirm the above observations, infected HMVEC-d cells were fixed, reacted with antibodies against viral capsid ORF65 protein and viral envelope glycoprotein gpK8.1A, and examined by immunofluorescent microscopy. The rationale was that if KSHV enters the target cells by fusion of virion envelope with the plasma membrane, then we will not observe any colocalization of viral envelope marker antibody with viral capsid marker antibody at a later time of infection. If KSHV enters by endocytosis, then we will observe colocalization of viral envelope with capsid. At 5 and 10 min p.i., the vast majority of KSHV capsid and envelope staining was colocalized (Fig. 1B, a to h), which suggests endocytosis of intact enveloped virus particles. We also observed occasional viral capsid staining independent of envelope at 5 min p.i., which increased at 10 min p.i. (Fig. 1B, d and h). These could represent free capsid in the cytoplasm, released from endocytic vesicles, and/or capsid entering the cytoplasm by fusion of viral envelope at the cell membrane. Taken together, the results of these morphological studies clearly indicate that KSHV utilizes endocytosis as one mode of entry into HMVEC-d cells.

Noncytotoxic concentrations of endocytosis inhibitors vary according to cell type. We have previously shown that KSHV enters HFF cells by clathrin-mediated endocytosis. Here, we used agents that are known to inhibit the various endocytic pathways to examine the mode of entry into HMVEC-d and HUVEC cells and compared the results with those of HFF cell infection. As an important prerequisite for these studies, we first determined the noncytotoxic concentrations of the various endocytic inhibitors used in the study (Table 1). The cytotoxic concentrations of the different inhibitors varied among the three primary cell types tested. HMVEC-d cells tolerated very low concentrations of the different inhibitors compared to HUVEC cells, while HFF cells tolerated comparatively higher concentrations of drugs than the endothelial cells (Table 1). For all subsequent studies, we used the noncytotoxic concentrations shown in Table 1.

Macropinocytosis inhibitors block KSHV gene expression in endothelial cells. Cells were pretreated for 1 h with nontoxic doses of inhibitors, washed, and infected with KSHV (10 DNA copies/cell), and viral gene expression levels at 2 h (lytic gene ORF50) and 24 h (latent gene ORF73) p.i. were measured by real-time RT-PCR (21). Chlorpromazine blocking of clathrin-mediated endocytosis did not have any effect on KSHV gene expression in HMVEC-d cells and, in contrast, inhibited more than 90% of viral gene expression in HFF cells (Fig. 2A and B). This suggests that KSHV entry in HMVEC-d cells is not through the clathrin-dependent pathway. Filipin, inhibiting the caveolar pathway, did not have any effect on KSHV infection of HMVEC-d and HFF cells (Fig. 2A and B). EIPA is a potent inhibitor of Na^+/H^+ exchangers, and rottlerin, a polycyclic aromatic compound derived from *Mallotus philippinensis*, is a selective inhibitor of fluid-phase endocytosis. Both of them have been shown to inhibit macropinocytosis. When HMVEC-d cells were treated with macropinocytosis inhibitors EIPA and rottlerin, ORF73 expression at 24 h p.i. was inhibited by about 67% and 61%, respectively, and ORF50 expression at 2 h p.i. was inhibited by about 63% and 53%, respectively (Fig. 2A). Interestingly, these inhibitors did not affect KSHV gene expression in HFF cells (Fig. 2B).

When HMVEC-d cells were treated with actin-depolymerizing cytochalasin D, the expression of KSHV ORF73 and ORF50 genes was inhibited by about 65% and 58%, respectively (Fig. 2A), and did not affect KSHV gene expression in HFF cells (Fig. 2B). Similar to the results of our earlier studies (43), in HMVEC-d cells treated with lipid raft-disrupting agents, such as MβCD, nystatin, and cholera toxin B, ORF73 expression was inhibited by about 88%, 83%, and 75%, respectively, while ORF50 expression was inhibited by about 67%, 88%, and 85%, respectively (Fig. 2A). These inhibitors did not affect KSHV infection of HFF cells (Fig. 2B). In HFF cells

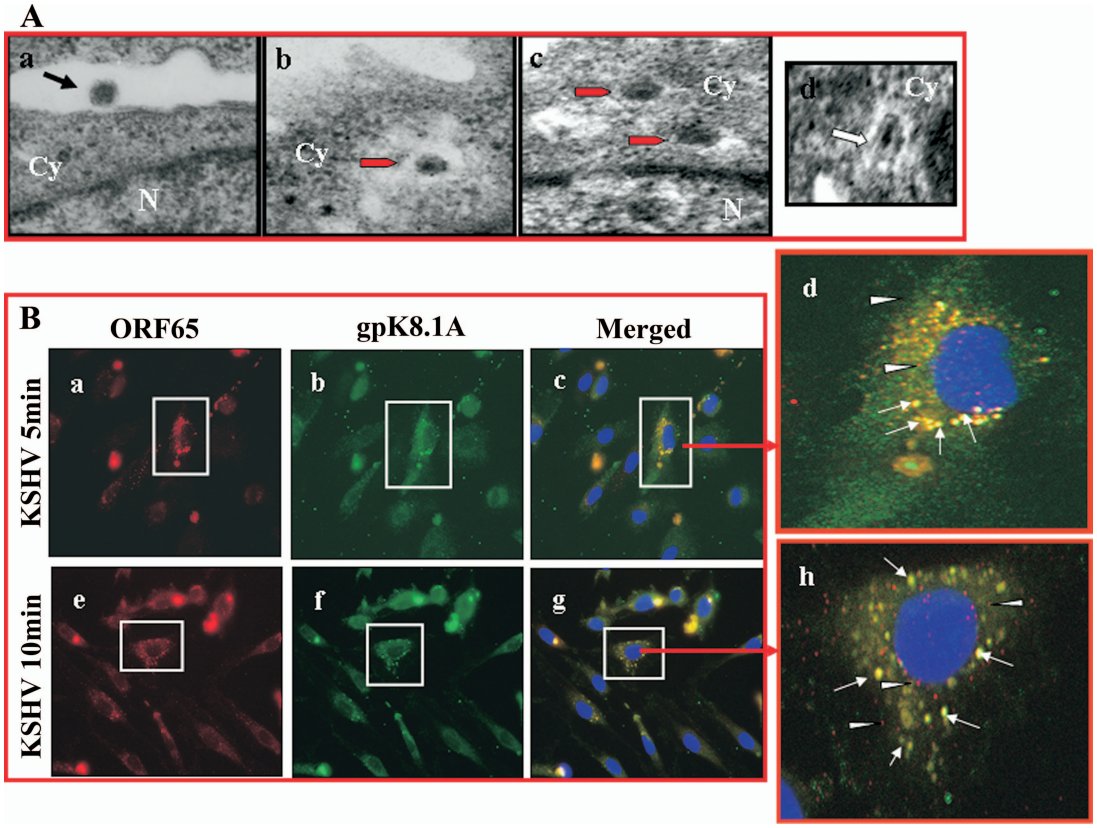

FIG. 1. Morphological observations of KSHV entry into HMVEC-d cells. (A) Electron microscopy of KSHV entry. HMVEC-d cells were incubated with purified KSHV at 37°C for different times, washed with PBS, and fixed in 2% glutaraldehyde. Thin sections were made for ultrastructural analysis by transmission electron micrography. Electron micrographs obtained at 5 min p.i. are shown here. Black arrow indicates a virus at the cell membrane. Red arrows indicate virion particles in endocytic vesicles. White arrow indicates a virion envelope in contact with endocytic vesicle membrane and in the process of fusion and release of the dark core. Magnifications: a, b, and c, ×64,000; d, ×82,000. Cy, cytoplasm; N, nucleus. (B) Immunofluorescence examination of KSHV entry. HMVEC-d cells grown in eight-chamber slides were infected with KSHV at an MOI of 10 (10 DNA copies/cell) for 1 h at 4°C and shifted to 37°C for the indicated times. Cells were fixed with 4% paraformaldehyde, permeabilized with 0.5% Triton X-100, blocked with 5% BSA, washed, and incubated with mouse anti-KSHV envelope glycoprotein gpK8.1A mAb and rabbit anti-KSHV capsid ORF65 protein immunoglobulin G antibody for 30 min at room temperature. After being washed, cells were incubated with anti-mouse Alexa Fluor 488 (green) and anti-rabbit Alexa Fluor 594 (red), respectively, for 30 min at room temperature, washed, mounted in DAPI, and visualized under a Nikon fluorescent microscope. The cell whose enlarged merged image is shown on the right is boxed in panels a to c and e to g (red arrow). White arrows indicate colocalization of ORF65 and gpK8.1A, and white arrowheads indicate free capsids. Magnification, ×80.

pretreated with 10 mM NH_4Cl, a weak lysomotropic base known to inhibit endosomal acidification, ORF73 expression was inhibited by about 91% and ORF50 expression was inhibited by about 92% (Fig. 2B). The toxicity of 1 mM or greater concentrations of NH_4Cl excluded their use in HMVEC-d cells. The specificity of reduction of viral gene expression in HMVEC-d cells by inhibitors of macropinocytosis, actin polymerization, and lipid rafts was demonstrated by the absence of inhibition in HFF cells.

These results suggest that macropinocytosis, actin polymerization, and lipid rafts play significant roles in KSHV infection of HMVEC-d cells. These results also validated our previous observations that KSHV enters HFF cells predominantly by clathrin-mediated endocytosis and requires a low-pH environment (1).

KSHV binding in HMVEC-d cells was not affected by inhibitors of macropinocytosis and actin polymerization. Inhibition of KSHV gene expression after treatment with inhibitors of macropinocytosis, actin polymerization, and lipid rafts could be due to interference in virus binding or viral DNA internalization or at the postentry steps, such as transport of virus capsid to the nucleus, delivery of viral DNA to the nucleus, and viral gene expression. Our earlier studies demonstrated that disruption of lipid rafts did not affect KSHV entry into HMVEC-d cells but inhibited nuclear delivery due to the disruption of phosphatidylinositol 3-kinase (PI3-K) and RhoA GTPases involved in microtubule aggregation and transport of viral capsid toward the nucleus (43). To determine whether inhibition in KSHV gene expression was due to KSHV's inability to bind endothelial cells, a radiolabeled-KSHV binding assay was carried out. KSHV binds to adherent and nonadherent cell surface heparan sulfate during the initial attachment stage of infection (4). Similar to earlier observations (1), preincubation of virus with 100 μg/ml of heparin inhibited >70% of [^{3}H]thymidine-labeled-KSHV binding to HMVEC-d cells (Fig. 2C). In contrast, there was no significant effect on KSHV

TABLE 1. Cytotoxicity analysis of endocytic inhibitors used in the study[a]

	HFF	HMVEC-d	HUVEC
Chlorpromazine (μg/ml)	5μg, 10μg, 20μg	2.5μg, 5μg, 7.5μg	2.5μg, 5μg, 10μg, 25μg, 50μg
EIPA (μg/ml)	2.5μg, 5μg, 10μg	0.25μg, 0.5μg, 1μg	0.25μg, 0.5μg, 1μg
Rottlerin (μM/ml)	5μM, 10μM, 20μM	1.5μM, 2.5μM, 5μM	1.5μM, 2.5μM, 5μM
Cytochalasin D (μg/ml)	2.5μg, 5μg, 10μg	0.5μg, 1μg, 1.5μg, 2.5μg	0.5μg, 1μg, 1.5μg, 2.5μg
Filipin (μg/ml)	0.5μg, 1μg, 2μg, 5μg	0.5μg, 1μg, 2μg	0.5μg, 1μg, 2μg, 5μg
CholeraToxin B (μg/ml)	25μg, 50μg, 100μg	25μg, 50μg, 100μg	25μg, 50μg, 100μg
MβCD (mM/ml)	5mM, 10mM, 20mM	2.5mM, 5mM, 10mM	1mM, 2.5mM, 5mM, 10mM
Nystatin (μg/ml)	25μg, 50μg, 100μg	25μg, 50μg, 100μg	25μg, 50μg, 100μg
NH4Cl (mM/ml)	5mM, 10mM, 20mM	1mM, 1.5mM, 2mM	25mM, 50mM, 100mM
LY294002 (μM/ml)	50μM, 100μM	50μM, 100μM	50μM, 100μM
Heparin (μg/ml)	100μg	100μg	100μg
Bafilomycin (nM/ml)		5nM, 10nM, 20nM	5nM, 10nM, 20nM
Dynasore (μM/ml)	50μM, 100μM	80μM, 100μM	80μM, 100μM

[a] Target cells were incubated with different concentrations of various inhibitors for 1 h and 4 h. Supernatants were collected and assessed for cellular toxicity by using a lactate dehydrogenase cytotoxicity assay kit. The concentrations marked in red represent the noncytotoxic concentration used in the study, while the concentrations marked in blue represent cytotoxic concentrations. The concentrations marked in black represent other noncytotoxic concentrations also used in the study.

binding with PI3-K inhibitor (LY294002), chlorpromazine, NH_4Cl, filipin, EIPA, rottlerin, or cytochalasin D (Fig. 2C). These results demonstrate that inhibition of KSHV viral gene expression after treatment with inhibitors of macropinocytosis and actin polymerization occurs at a postbinding stage of infection.

Inhibition of macropinocytosis and actin polymerization inhibits KSHV entry in HMVEC-d cells. To determine whether the reduction in KSHV gene expression in HMVEC-d cells was due to interference in viral entry, total viral DNA internalization (cytoplasmic and nuclear) was measured by real-time DNA PCR. The percent inhibition of KSHV DNA internalization obtained when the cells were incubated with virus alone was calculated. As reported in our earlier studies (43), we observed about 70% to 80% reduction in viral DNA internalization in HMVEC-d and HFF cells from preincubating virus with heparin or from pretreating cells with PI3-K inhibitor LY294002 (Fig. 2D and E). No significant inhibition in internalization was observed from preincubating HMVEC-d cells with chlorpromazine (Fig. 2D), and in contrast, about 65% inhibition of KSHV internalization in HFF cells was observed with the 10-μg concentration of chlorpromazine (Fig. 2E). No inhibition of KSHV entry was observed in filipin- and NH_4Cl-treated HMVEC-d and HFF cells (Fig. 2D and E). We observed about 45% to 50% inhibition in KSHV internalization in HMVEC-d cells pretreated with 0.250 μg of EIPA, 2.5 μM rottlerin, or 1 μg of cytochalasin D (Fig. 2D) and no effect in HFF cells (Fig. 2E). We also observed a dose-dependent inhibition of viral DNA entry with various concentrations of EIPA, rottlerin, and cytochalasin D (data not shown).

During the early stages of HMVEC-d and HFF cell infection, KSHV induces the aggregation of microtubules via Rho GTPase-induced acetylation and utilizes the microtubules to transport its capsids toward the infected cells' nuclei (32, 43). As observed before (43), at 30 min p.i., in the absence of drug treatment, we observed abundant association of KSHV capsids with microtubules which was distributed more toward the nucleus (Fig. 3, a to d). In contrast, we did not observe any significant colocalization of KSHV capsids with the aggregated microtubules in HMVEC-d cells pretreated with 0.250 μg of EIPA (Fig. 3, e to h). Instead, the majority of the viral capsids were distributed at the periphery of the infected cells, presumably at the plasma membranes, and this observation was interpreted as an indication of a block in KSHV entry (Fig. 3, e to h).

Taken together, these results suggested that macropinocytic and actin polymerization inhibitors could be exerting their effects predominantly at the entry stage of KSHV infection of HMVEC-d cells.

KSHV infection of HMVEC-d cells induces actin polymerization that is involved in macropinocytosis. Macropinocytosis involves the formation of lamellipodia, or ruffles, which are curtain-like plasma membrane extensions formed by the polymerization of actin filaments along the edge of the cells (18). Actin polymerization is controlled by the Rho family of small GTPases, such as Rho, Rac, and Cdc42 (35, 36). Activated Rac regulates the formation of lamellipodia, and activated Rho mediates the formation of stress fibers, elongated actin bundles that traverse the cells and promote cell attachment to the extracellular matrix (35, 36). Activated Cdc42 induces the formation of filopodia, thin finger-like extensions containing actin bundles, and these GTPases are activated by PI3-K (35, 36). In our earlier studies with HFF cells, we demonstrated that within minutes of infection, KSHV induces PI3-K, Rho GTPases, and actin polymerization; formation of stress fibers, filopodia, and lamellipodia; and microtubule acetylation and aggregation (31, 32).

KSHV's ability to induce PI3-K and Rho GTPases in HMVEC-d cells (43), coupled with the above results indicating macropinocytosis as one of the pathways of KSHV entry in HMVEC-d cells, prompted us to examine the actin cytoskeleton changes in infected cells. Uninfected cell surfaces were smooth and showed a clear margin with peripheral F-actin staining (Fig. 4A and B, a). KSHV induced the formation of stress fibers, filopodia, and lamellipodia as early as 5 min p.i. in HMVEC-d and HUVEC cells, and lamellipodia were observed as clear extensions from the cell surface (Fig. 4A and B, b and c). These results demonstrated that early during infection, KSHV induced the formation of actin polymerization-dependent lamellipodial extensions that are essential for macropinocytosis.

Inhibition of macropinocytosis and actin polymerization inhibits KSHV entry in HUVEC cells. HUVEC cells have been used as a target cell for KSHV in many studies (7, 13, 37, 65). To determine the mode of KSHV entry into HUVEC cells, we examined the kinetics of KSHV entry, nuclear delivery, and gene expression during the early stages of infection. Similar to the results for HMVEC-d and HFF cells (21), we observed rapid internalization of KSHV DNA in HUVEC cells (Fig. 5A). Internalized viral DNA could be detected in HUVEC cells as early as 5 min p.i., with the level increasing steadily over the 240-min period of observation (Fig. 5A). Real-time DNA PCR analysis of DNA from the infected-cell nuclei demon-

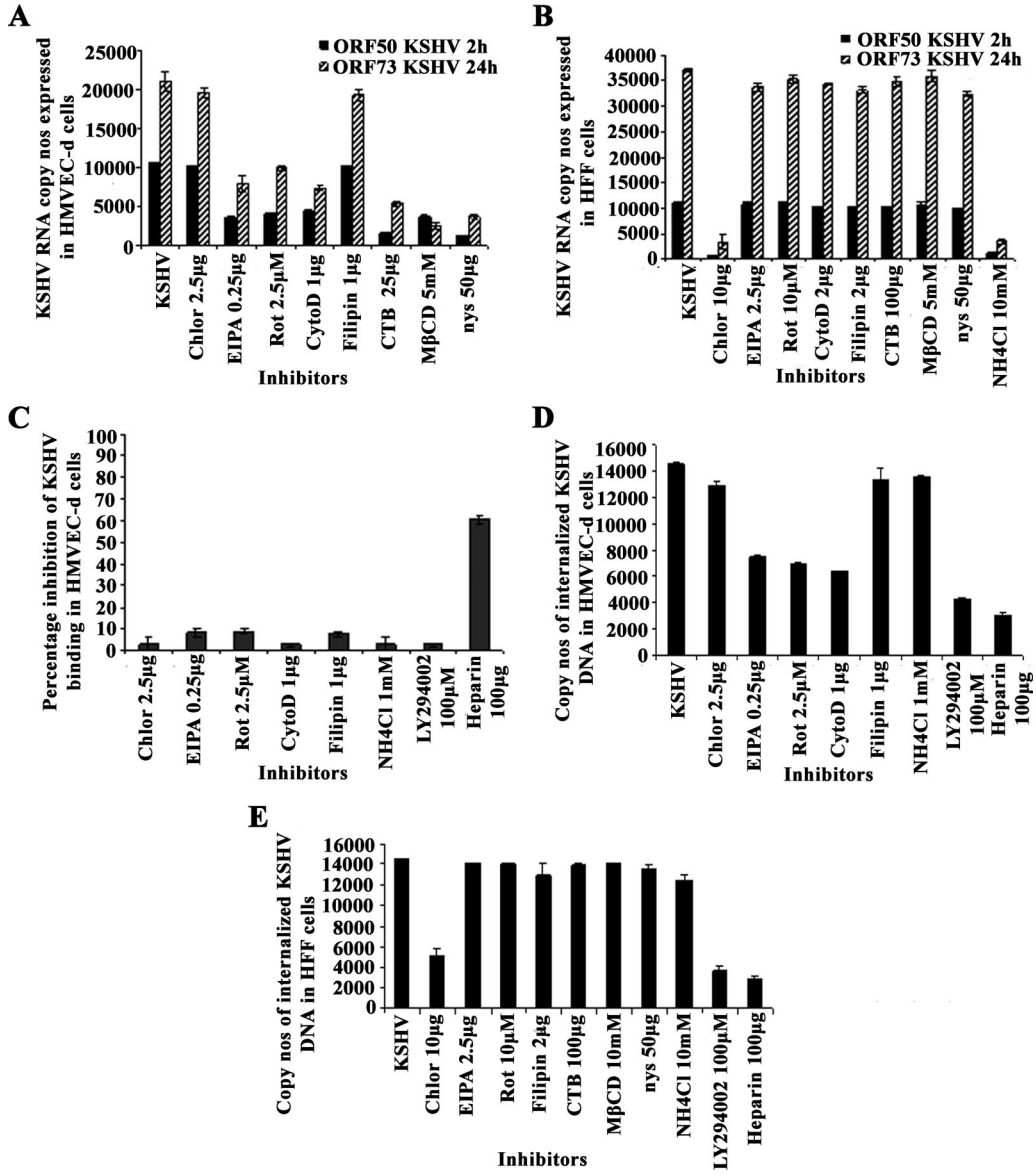

FIG. 2. Effect of endocytic inhibitors on KSHV gene expression, binding, and entry in HMVEC-d and HFF cells. (A and B) Cells were left untreated or pretreated with endocytic inhibitors for 1 h at 37°C, washed, and infected with KSHV at an MOI of 10. Total RNA was isolated at 2 h and 24 h p.i., and 50 ng of DNase-treated RNA/μl was subjected to real-time RT-PCR with ORF73 and ORF50 gene-specific primers and TaqMan probes. Known concentrations of DNase-treated, in vitro-transcribed ORF50 and ORF73 transcripts were used in real-time RT-PCR to construct a standard graph from which the relative copy numbers of viral transcripts were calculated and normalized to the amount of GAPDH. Histograms depict KSHV ORF73 and ORF50 gene RNA copy numbers in untreated cells (KSHV) or cells in the presence of indicated nontoxic concentrations of chlorpromazine (Chlor), EIPA, rottlerin (Rot), cytochalasin D (CytoD), filipin, cholera toxin B (CTB), MβCD, or nystatin (nys) in HMVEC-d (A) and HFF (B) cells. Each reaction was done in duplicate, and each bar represents the mean ± standard deviation of the results of three independent experiments. (C, D, and E) Effect of endocytic inhibitors on KSHV binding (C) and internalization (D) in HMVEC-d cells and on internalization (E) in HFF cells. (C) HMVEC-d cells grown in 24-well plates were either left untreated or pretreated with various nontoxic concentrations of agents for 1 h at 37°C and incubated with a fixed concentration of [^{3}H]thymidine-labeled virus for 1 h at 4°C. As a control, labeled KSHV was preincubated with 100 μg of heparin/ml for 1 h at 37°C before being added to the cells. After incubation, cells were washed, lysed, and precipitated with trichloroacetic acid and the cell-associated-virus radioactivity (in cpm) was counted. The cell-associated cpm in the presence of drugs compared to virus binding to untreated cells was calculated as the percent inhibition of virus binding. Each reaction was done in triplicate, and each bar represents the average ± standard deviation of the results of three independent experiments. (D and E) Cells grown in six-well plates were either left untreated or preincubated with drugs at 37°C for 1 h. Cells were incubated with KSHV for 2 h, washed to remove unbound virus, treated with trypsin-EDTA for 5 min at 37°C to remove unbound, noninternalized virus, and washed, and the total DNA was isolated. KSHV preincubated with 100 μg of heparin/ml for 1 h at 37°C before being added to the cells was used as a control. KSHV ORF73 DNA copy numbers were estimated by real-time DNA PCR (21). Each reaction was done in duplicate, and each bar represents the mean ± standard deviation of the results of three experiments.

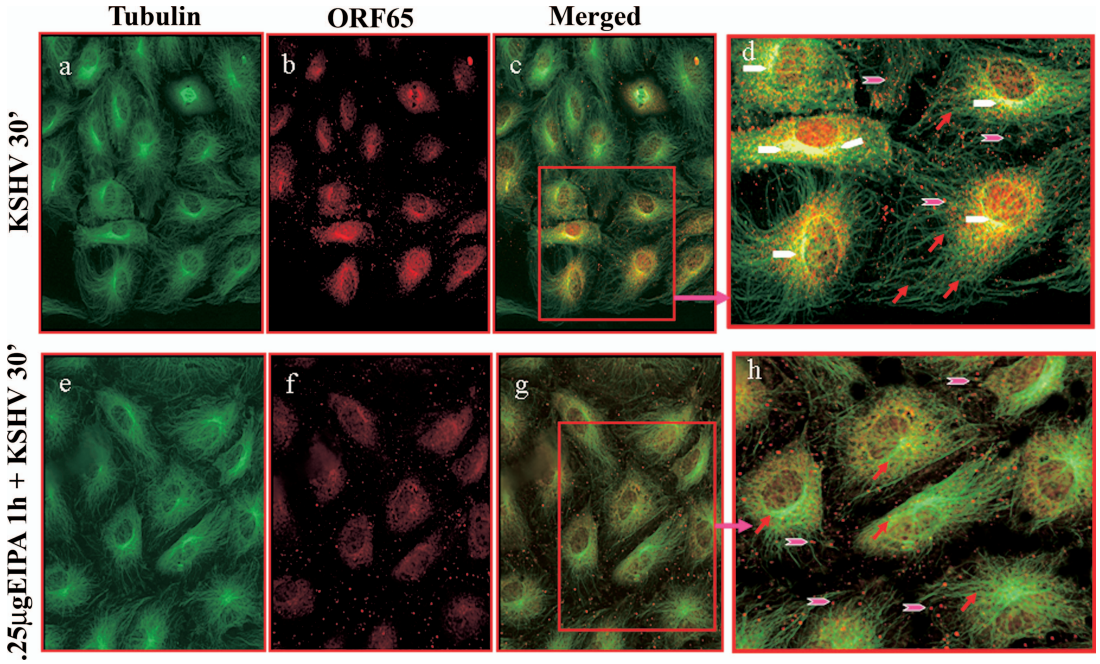

FIG. 3. KSHV trafficking after treatment with macropinocytic inhibitor EIPA. HMVEC-d cells grown in eight-chamber slides were left untreated or treated with 0.25 μg EIPA, washed, infected with KSHV at an MOI of 100 for 30 min (30′) at room temperature, washed, fixed, permeabilized, blocked in 5% BSA, incubated in BSA with primary antibodies to tubulin and KSHV capsid ORF65 protein for 1 h at room temperature, washed, incubated with secondary antibodies to tubulin (green) and ORF65 (red), washed, mounted, and viewed under an immunofluorescence microscope. Pink arrowheads indicate KSHV capsids, red arrows indicate tubulin, and white arrowheads indicate colocalization of KSHV capsids with microtubules. Magnification, ×80. Boxed areas in c and g are shown enlarged in d and h.

strated the association of KSHV DNA with infected-cell nuclei as early as 5 min p.i., with the level increasing steadily over 240 min p.i. (Fig. 5B). In HMVEC-d and HFF cells, primary KSHV infection resulted in the transient expression of limited lytic cycle genes, including the lytic cycle switch gene ORF50, and persistent expression of latent genes (21). During primary KSHV infection of HUVEC cells, we observed a high level of ORF50 gene expression, which peaked at 8 h p.i. and declined sharply thereafter (Fig. 5C). The expression of the early lytic K8 gene and the late lytic gpK8.1 gene was 60-fold lower than the ORF50 gene expression and did not increase over time (Fig. 5C). In contrast, expression of the latent ORF73 gene was detected as early as 2 h p.i. and increased steadily during the observed 72 h p.i. (Fig. 5C). These results suggested that the expression kinetics of latent and lytic genes in KSHV infection of HUVEC cells follow a pattern very similar to that of primary infection of HMVEC-d and HFF cells.

To determine whether KSHV enters HUVEC cells by endocytosis, we pretreated the cells with nontoxic concentrations of inhibitors of endocytosis for 1 h at 37°C, infected them with KSHV for 2 h, and examined ORF73 and ORF50 expression at 48 h and 8 h p.i., respectively (Fig. 5D). Similar to the results for HMVEC-d cells, chlorpromazine, which blocks clathrin-mediated endocytosis, and filipin, a caveolar pathway inhibitor, did not have any effect on KSHV gene expression in HUVEC cells (Fig. 5D). In cells treated with the macropinocytosis inhibitor EIPA, ORF50 and ORF73 expression was inhibited by about 95% and 92%, respectively (Fig. 5D), while rottlerin inhibited ORF50 and ORF73 expression by about 85% and 68%, respectively (Fig. 5D). In cytochalasin D-treated HUVEC cells, expression of ORF50 and ORF73 was inhibited by about 72% and 58%, respectively (Fig. 5D). In contrast to the results for HMVEC-d cells, lipid raft-disrupting MβCD, nystatin, and cholera toxin B did not show any significant inhibition of KSHV gene expression in HUVEC cells (Fig. 5D). These results suggest that macropinocytosis and actin polymerization play significant roles in KSHV infection of HUVEC cells. When we examined viral DNA internalization in HUVEC cells treated with various inhibitors, KSHV internalization was inhibited by pretreating cells with macropinocytic inhibitors (50% to 60%), cytochalasin D (38%), and PI3-K inhibitor LY294002 (65% to 70%) and by preincubating virus with heparin (70%) (Fig. 5E). Taken together, these results suggest that KSHV utilizes macropinocytosis as one of its predominant pathways for infectious entry into HUVEC cells.

KSHV colocalizes with macropinocytosis marker dextran in endothelial cells. Since dextran has been used as a marker for macropinocytosis (16, 18, 27), cells were incubated with Texas Red-labeled dextran and KSHV at 37°C for different times. Dextran uptake was observed in uninfected endothelial cells (Fig. 6A, a to d). When we examined the infected HMVEC-d and HUVEC cells for KSHV with anti-gpK8.1A mAb, we observed the colocalization of KSHV with dextran as early as 5 min p.i., as well as at 10 and 15 min p.i. (Fig. 6A, e to p, and D, e to l). In contrast, we did not observe any colocalization of KSHV with the clathrin pathway marker transferrin either in HMVEC-d (Fig. 6B, eto p) or in HUVEC (Fig. 6E, a to d) cells. In addition, we did not observe any colocalization of KSHV with caveolin in HMVEC-d cells (Fig. 6C, e to p) or in HUVEC cells (data not shown). These results further confirm

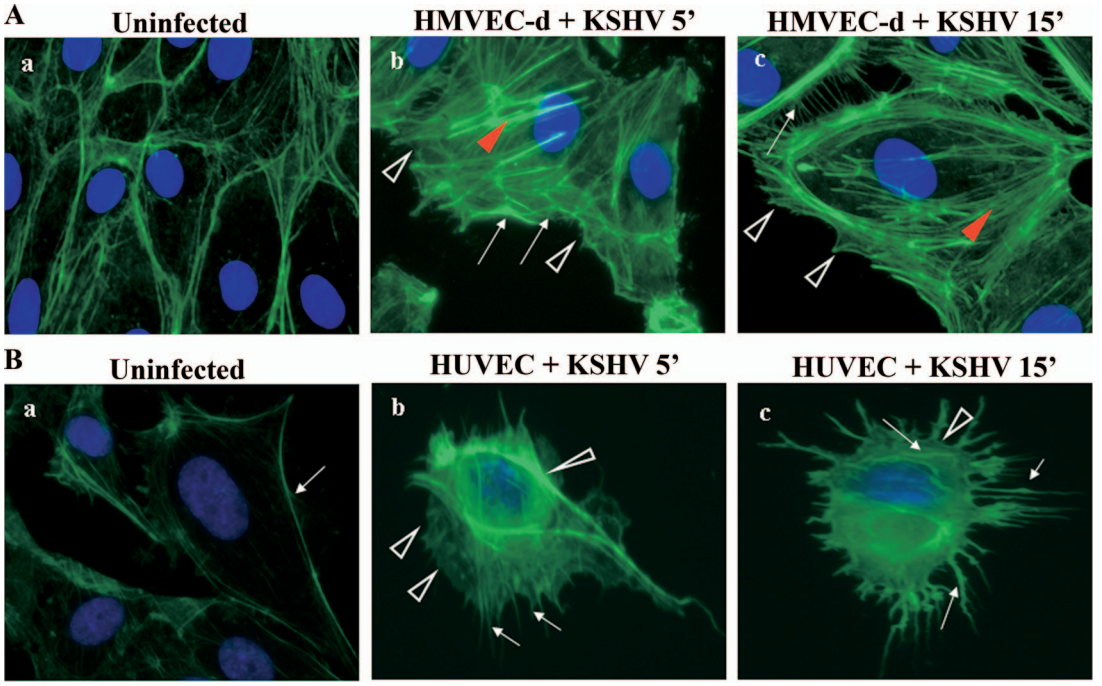

FIG. 4. KSHV induces actin polymerization in HMVEC-d (A) and HUVEC (B) cells. HMVEC-d and HUVEC cells were left uninfected or infected with KSHV (MOI of 10) at 37°C for different times (', min), fixed, permeabilized, and stained for polymerized actin by using Alexa Fluor 488-labeled phalloidin for 30 min at room temperature. Red arrowheads indicate the accumulated actin stress fibers, white arrows indicate hair-like membrane filopodial extensions, and white arrowheads indicate sites of membrane ruffling. Magnification, ×40.

that in HMVEC-d and HUVEC cells, KSHV utilizes macropinocytosis as a predominant mode of entry.

KSHV entry into endothelial cells is dynamin independent. Dynamin, a 100-kDa cytosolic small GTPase, plays a crucial role in endocytosis by releasing the internalized endocytic vesicles from the plasma membrane. Dynamin associates with clathrin-coated and other membrane invaginations and functions in several endocytic scission events, including the clathrin-coated vesicle, formation of caveolae, budding of Golgi complex-derived vesicles, phagocytosis, and nonclathrin-mediated endocytosis. Macropinocytosis and other types of endocytosis have been shown to be independent of dynamin (5). To determine whether the macropinocytic entry of KSHV into HMVEC-d and HUVEC cells is dependent on dynamin, we transfected the cells with plasmids Dyn-WT and dyn-K44A (kind gift from Mark McNiven, Mayo Clinic, Rochester, MN) and normalized the data by blotting for GFP expression (data not shown). Protein coded by plasmid dyn-K44A fails to load GTPase, and this dominant-negative mutant form of dynamin has been shown to block clathrin-mediated endocytosis of transferrin and epidermal growth factors. We observed about 30% to 40% transfection efficiency in HMVEC-d cells (Fig. 7A, a to d). We did not observe any change in KSHV DNA internalization in HMVEC-d cells transfected with the WT dynamin and K44A plasmids (Fig. 7B). These results suggested that the macropinocytic pathway observed in HMVEC-d cells is dynamin independent.

To further strengthen this observation, we used dynasore, a cell-permeable inhibitor of dynamin 1 and dynamin 2, and tested its effect on KSHV internalization in HMVEC-d, HUVEC, and HFF cells. In HUVEC (Fig. 7C) and HMVEC-d (Fig. 7D) cells, we did not observe any change in KSHV internalization after pretreatment with dynasore. In contrast, we observed about 50% inhibition of KSHV entry at 5 and 10 min p.i. in HFF cells (Fig. 7E). These results suggested that KSHV enters HFF cells by a dynamin-dependent pathway but enters HMVEC-d and HUVEC cells by a dynamin-independent pathway.

Trafficking of KSHV-containing macropinosomes in HMVEC-d cells does not involve early endosomes but involves late endosomes. To study the trafficking of the macropinosome and to determine whether it involves the early and late endosomes, we examined the association of KSHV with the classical early endocytic marker EEA-1 and late endosome marker LAMP-1 at different time points p.i. KSHV-infected HMVEC-d cells were fixed at different times p.i. and were examined for the association of EEA-1 and LAMP-1 with viral capsid protein ORF65. When uninfected cells were incubated with transferrin for 5 min as control, transferrin receptor, which is known to be endocytosed by clathrin-mediated endocytosis, colocalized with EEA-1 (Fig. 8A, a to f and enlargements). In contrast, we did not observe any colocalization of KSHV capsids with EEA-1 at 10, 30, and 60 min p.i. Representative results at 10 and 30 min p.i. are shown in Fig. 8B, a to f and enlargements. In contrast, we observed maximum colocalization of viral capsids with LAMP-1 (late endosomes) at 30 min p.i. (Fig. 8C, a to c and enlargement). Minimal colocalization of viral capsids with LAMP-1 was also observed at 60 min p.i. (Fig. 8C, d to f and enlargement). These results suggested that intracellular trafficking of KSHV-containing macropinosomes does not involve early endosomes but involves late endosomes.

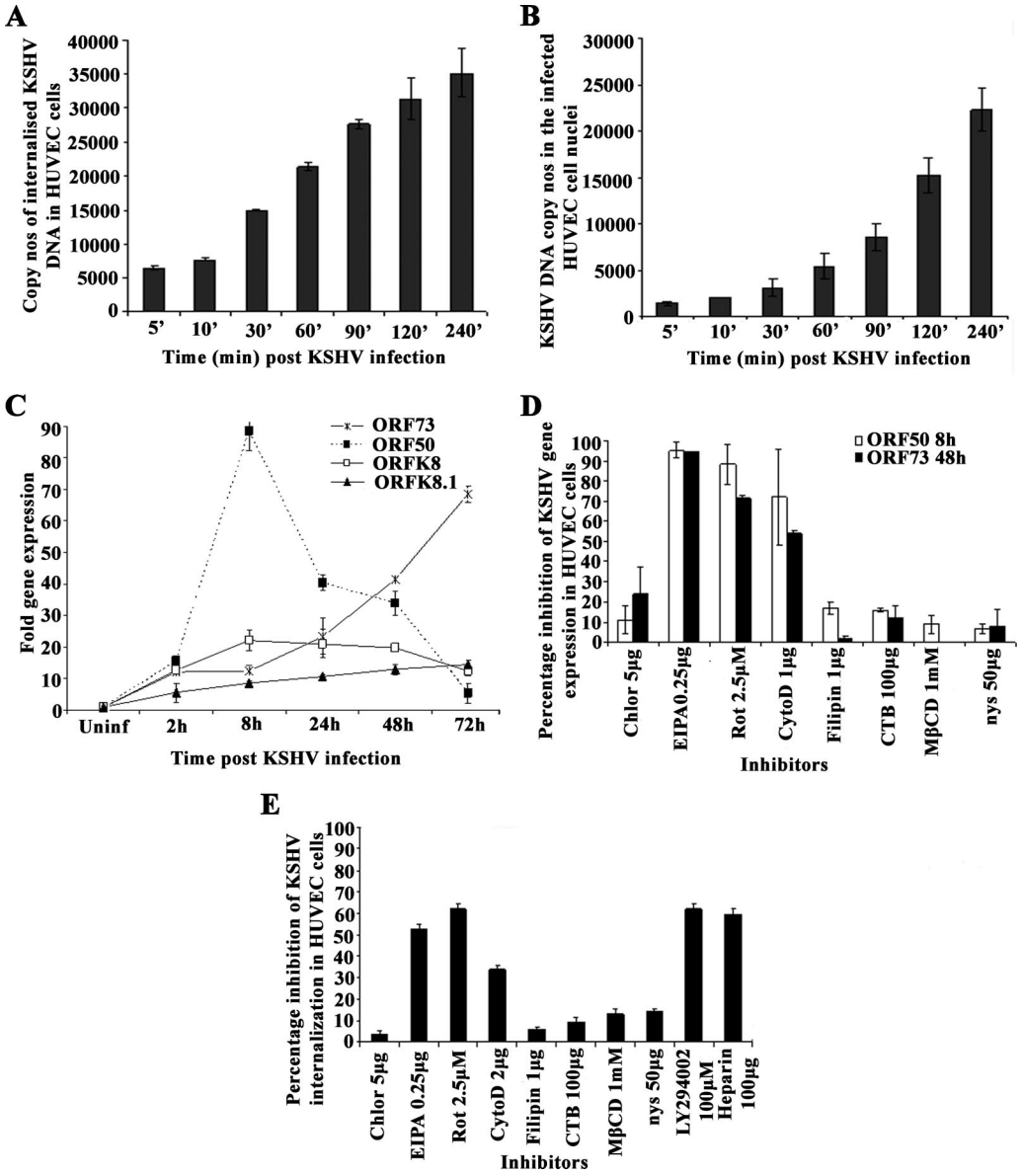

FIG. 5. Effects of endocytic inhibitors on KSHV entry into HUVEC cells. (A) Kinetics of KSHV entry into HUVEC cells. HUVEC cells were infected with KSHV (100 DNA copies per cell), and amounts of internalized viral DNA at different time points were estimated as described in the Fig. 2D and E legend. Each reaction was done in duplicate, and each bar represents the mean ± standard deviation of the results of three experiments. (B) Kinetics of KSHV DNA delivery into infected-cell nuclei. Nuclear fractions from HUVEC cells infected with KSHV at 100 DNA copies per cell for the indicated times (', min) were isolated, and total DNA extracted, normalized to 100 ng/5 μl, and analyzed by real-time DNA PCR with KSHV ORF73 primers. Each reaction was done in duplicate, and each bar represents the mean ± standard deviation of the results of three experiments. (C) Kinetics of KSHV latent gene (ORF73) and lytic gene (ORF50, K8, and gpK8.1) expression in HUVEC cells. For RNA isolation, PCR primers, and methodology, refer to Materials and Methods. Each sample was measured in triplicate, and data were analyzed by the threshold cycle method for comparing relative expression results. For each experiment, PCR amplifications without cDNA were performed as negative controls. (D) Effect of endocytic inhibitors on KSHV gene expression in HUVEC cells. HUVEC cells grown in six-well plates were either left untreated or preincubated with various nontoxic concentrations of agents for 1 h at 37°C, washed, and incubated with KSHV for 2 h, and total RNA was isolated at 8 h and 48 h p.i. and subjected to real-time RNA PCR. Histogram depicts the percent inhibition in KSHV ORF73 and ORF50 gene RNA copy numbers in the presence of indicated drugs, obtained by comparison with copy numbers in cells incubated with virus alone. Each reaction was done in duplicate, and each bar represents the mean ± standard deviation of the results of three experiments. (E) Effect of endocytic inhibitors on KSHV internalization in HUVEC cells. HUVEC cells grown in six-well plates were either left untreated or preincubated with various nontoxic concentrations of agents at 37°C for 1 h and infected with KSHV for 2 h, and the amount of internalized viral DNA at different time points was estimated as described in the Fig. 2D and E legend. The data are represented as the percent inhibition of KSHV DNA internalization in comparison with that in cells incubated with virus alone. Each reaction was done in duplicate, and each bar represents the mean ± standard deviation of the results of three experiments. Chlor, chlorpromazine; Rot, rottlerin; CytoD, cytochalasin D; CTB, cholera toxin B; nys, nystatin.

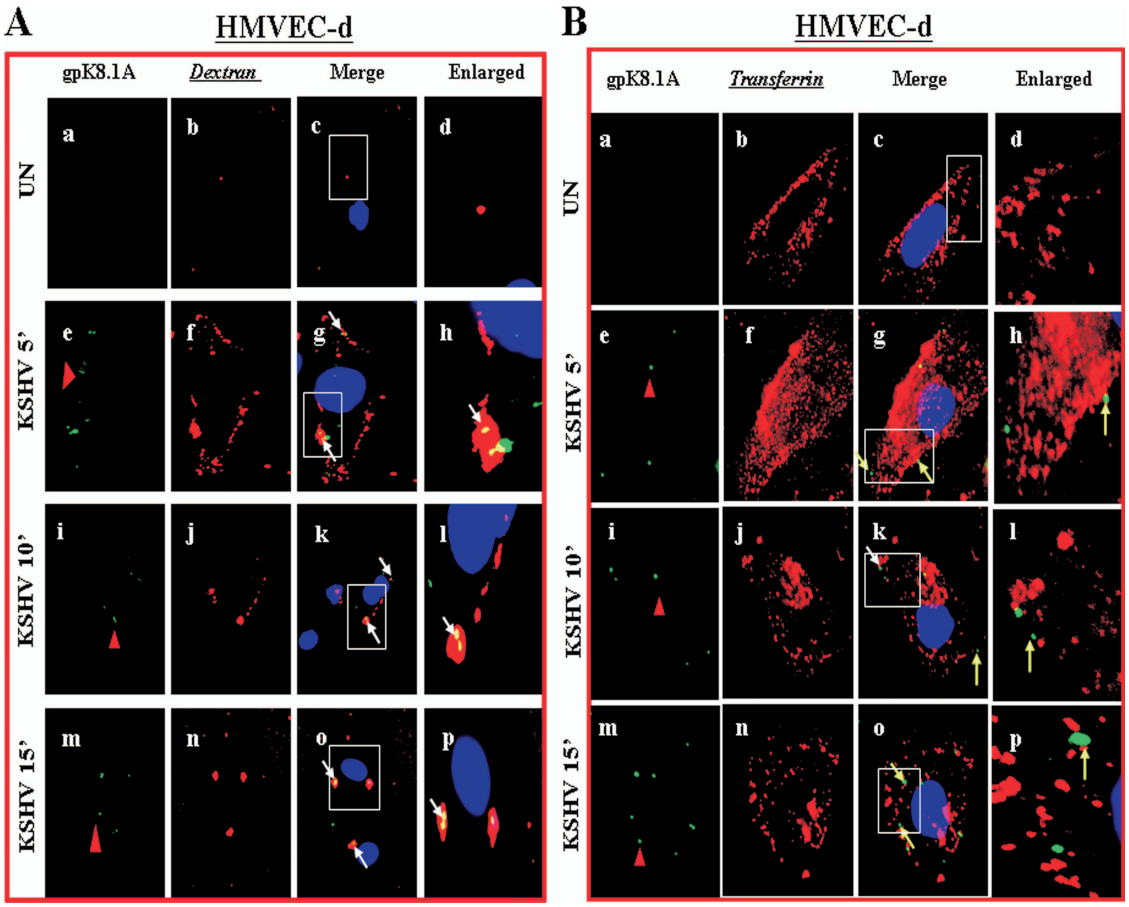

FIG. 6. KSHV colocalizes with macropinocytic marker dextran and not with transferrin and caveolin. (A and D) Colocalization of KSHV with dextran. Uninfected and infected HMVEC-d (A) and HUVEC (D) cells were incubated at 37°C with Texas Red-labeled dextran and KSHV for 5, 10, and 15 min. Cells were washed in HBSS, fixed with 2% paraformaldehyde, permeabilized with 0.2% Triton X-100, blocked in 5% BSA, and then incubated with anti-gpK8.1A mAb followed by Alexa Fluor 488-labeled goat anti-mouse secondary antibody. Magnification, ×40. White arrows indicate colocalization of KSHV with dextran. (B and E) KSHV does not colocalize with transferrin. Uninfected cells and cells infected with KSHV and Alexa Fluor 594-conjugated transferrin were examined with anti-gpK8.1A antibody. Magnification, ×40. Yellow arrows indicate virus particles not colocalized with transferrin. (C) KSHV does not colocalize with caveolin. Uninfected and infected cells were incubated with anti-gpK8.1A and anticaveolin antibodies for 1 h at room temperature. The staining was visualized by incubation with Alexa Fluor 488-labeled antibody for gpK8.1A and Alexa Fluor 594-labeled secondary antibody for caveolin. Magnification, ×40. Yellow arrows indicate virus particles not colocalized with caveolin. Boxed areas are shown enlarged in the right-hand panels. ', min; UN, uninfected.

Trafficking of KSHV-containing macropinosomes in HMVEC-d cells involves Rab34 GTPase. The trafficking and fusion of endosomes is controlled by Rab GTPases which act as molecular switches and play important roles in the formation and movement of endocytic vesicles (40, 56). Rab34 GTPase is implicated in macropinocytosis and has been shown to be associated with the formation of efficient macropinosomes from the sites of membrane ruffling (48). Our earlier studies have demonstrated that inhibition of Rho GTPases inhibited KSHV entry, as well as its migration toward the infected-cell nuclei of HFF and HMVEC-d cells (32, 43). To determine whether Rab34 GTPase plays a role in KSHV entry, we examined the infected HMVEC-d cells at different times p.i. with anti-Rab34 antibodies and with anti-gpK8.1A antibody as the viral marker. Thin sections representing z-stacks were made at different time points p.i., and one representative section through the middle of the stack is shown (Fig. 9A, f, i, and l). As early as 10 min p.i., we observed the association of KSHV gpK8.1A with Rab34 by confocal microscopy (Fig. 9A, d to f), and colocalization was also observed at 30 and 60 min p.i. (Fig. 9A, g to i and j to l). The results of these studies suggest that KSHV-containing macropinosomes are probably regulated through Rab34 GTPases.

To determine the role of Rab34 GTPases in KSHV infection, we utilized gene silencing techniques. In HMVEC-d cells transfected with si-Rab34, we observed about 58% and 59% reduction in Rab34 expression at 24 h and 48 h, respectively, compared to that in si-C-transfected HMVEC-d cells (Fig. 9B). At 24 h posttransfection of si-C and si-Rab34, HMVEC-d cells were infected with KSHV at an MOI of 10, and ORF73 and ORF50 gene expression was analyzed at different times p.i. Compared to si-C-transfected HMVEC-d cells, KSHV ORF73 gene expression in the si-Rab34-transfected HMVEC-d cells was reduced by about 56%, 39%, and 53% at 2 h, 8 h, and 24 h p.i, respectively (Fig. 9C). Transfection of si-Rab34 in HMVEC-d cells also decreased KSHV ORF50 gene expres-

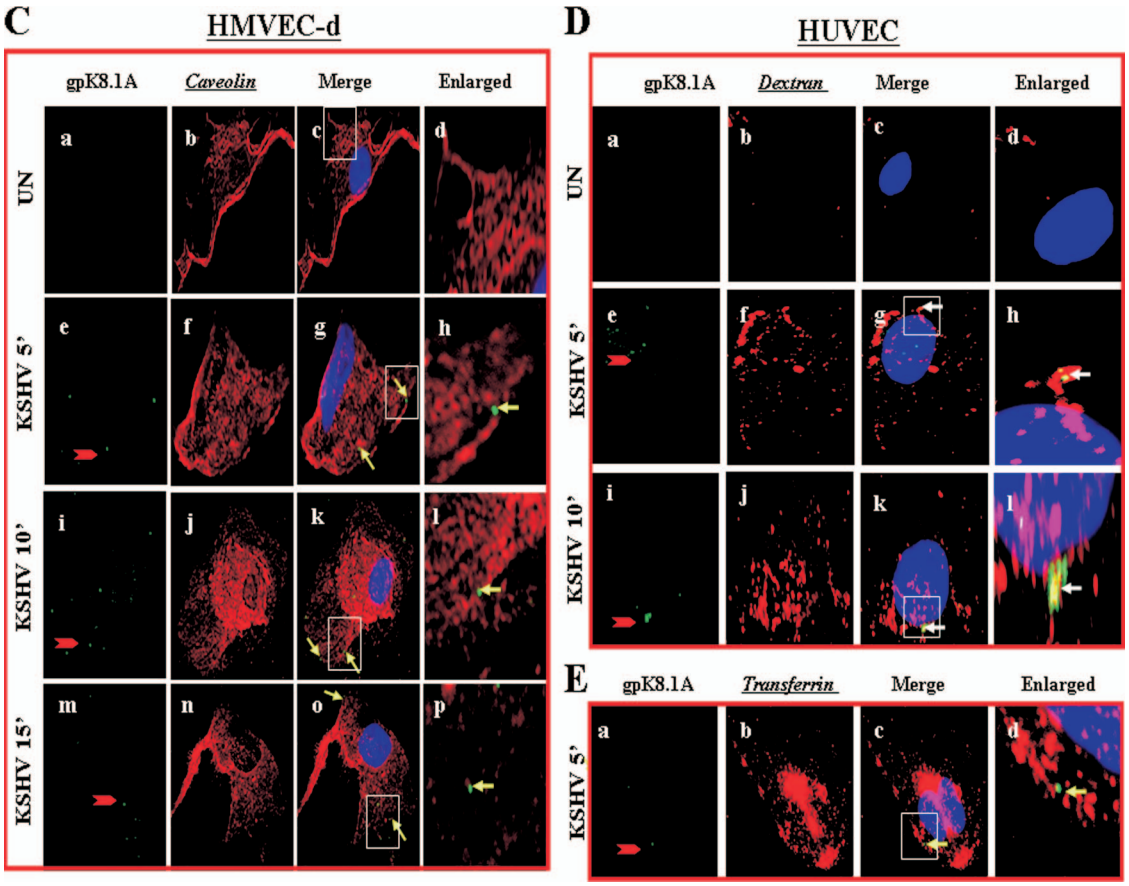

FIG. 6—*Continued.*

sion by about 43%, 61%, and 55% at 2 h, 8 h, and 24 h, respectively (Fig. 9C). These results clearly demonstrate that Rab34 GTPase plays a critical role in KSHV infection, presumably by its role in macropinocytosis.

KSHV infection of endothelial cells requires acidification of macropinosomes. Bafilomycin is a specific and potent inhibitor of vacuolar H^+ ATPase, resulting in inhibition of endosome and lysosome acidification. When cells were pretreated with 20 nM of bafilomycin before infection, KSHV ORF73 and ORF50 gene expression was inhibited by about 50% and 48% in HMVEC-d cells, respectively (Fig. 10A). In HUVEC cells, both NH_4Cl and bafilomycin inhibited about 90% of ORF50 expression at 8 h p.i., while 55 to 65% inhibition was observed in ORF73 gene expression at 48 h after treatment with the endosomal acidification inhibitors (Fig. 10B). These results suggested that in both HMVEC-d and HUVEC cells, KSHV utilizes a low-pH environment for its infectious entry.

DISCUSSION

Various studies have shown that herpesviruses enter their in vitro target cells either by fusion of their envelope with the plasma membrane or by endocytosis followed by fusion of their envelope with the endosome membrane (17, 20, 33, 34, 54, 63). Endocytosis is utilized by many enveloped and nonenveloped viruses to enter target cells, as endosomes offer a convenient and often rapid passage across the plasma membrane and through a crowded cytoplasm, as well as for the delivery of viral capsid to the vicinity of the nuclear pore for viruses replicating their genome in the nucleus (24, 52, 66). KSHV utilizes endocytosis as a mode of entry to infect HFF, BJAB, HEK 293, and activated primary human B cells (1, 4, 44). In this report, we have presented several lines of evidence that the dynamin-independent macropinocytic pathway, involving the late endosome and low-pH environment, is used as a predominant method of KSHV entry into human endothelial (HMVEC-d and HUVEC) cells. Our observations suggest that KSHV does not utilize clathrin and caveolar pathways, and the reduction of viral gene expression by about 60% to 65% by EIPA and rottlerin clearly demonstrated that KSHV entry into endothelial cells via macropinocytosis results in a productive infection. Although we did not observe fusion of KSHV at the plasma membrane, we cannot rule out this mode of entry, and macropinocytosis could be one of the major pathways of entry into endothelial cells.

Viruses may use multiple pathways to enter target cells, and some pathways may predominate over others. For example, after interaction with CD4 and chemokine receptor molecules, human immunodeficiency virus type 1 enters susceptible cells by fusion of its envelope with the plasma membrane; however, the virus enters brain endothelial cells by macropinocytosis after engaging heparan sulfate and other receptors, which de-

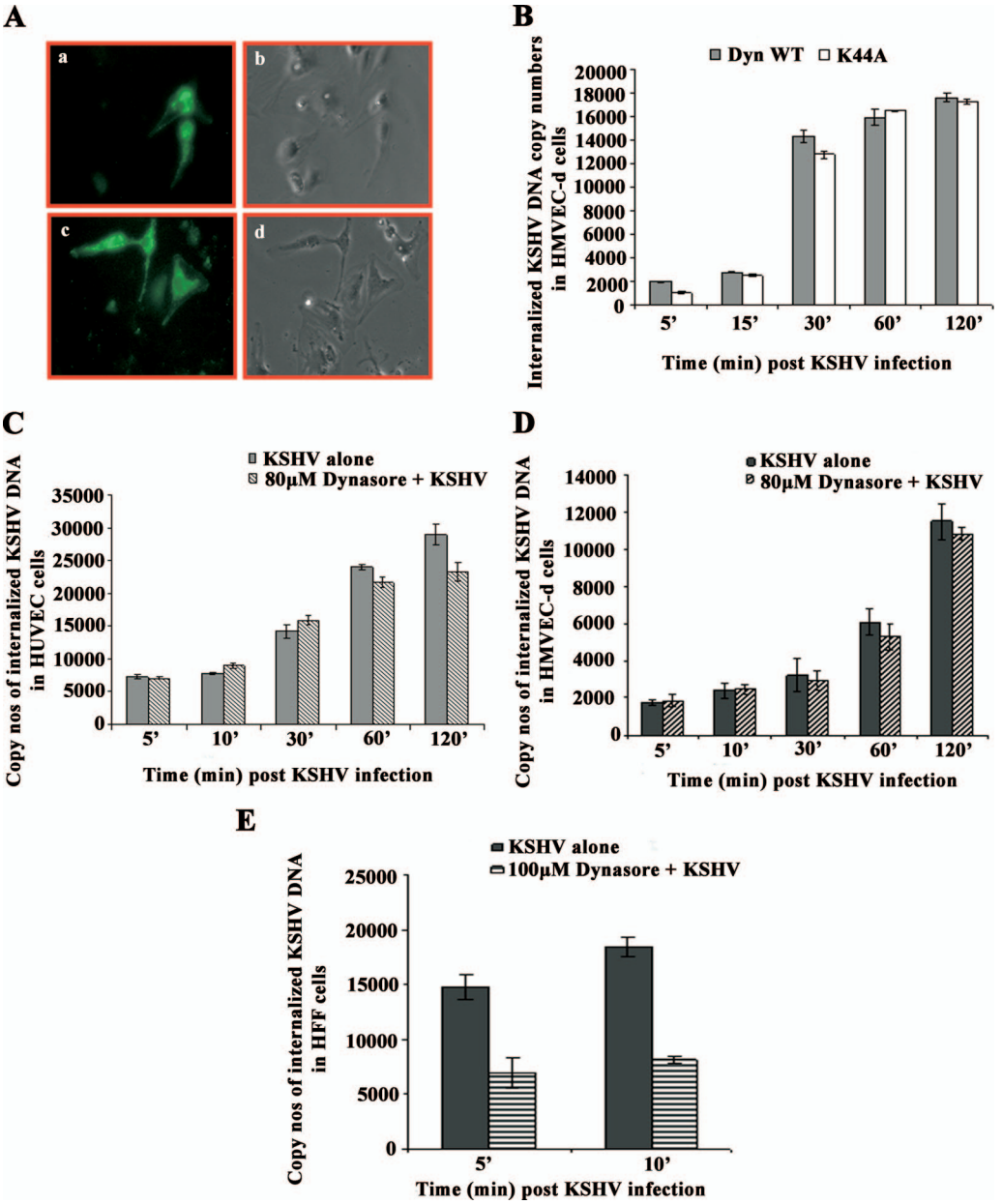

FIG. 7. KSHV entry in HMVEC-d and HUVEC cells is dynamin independent. (A) HMVEC-d cells showing transfection with WT dynamin. Cells were transfected with 1 μg of GFP-WT dynamin plasmid or 1 μg of GFP-K44A dynamin plasmid and observed under a microscope after 24 h. a and c, GFP; b and d, phase-contrast microscopy. Magnification, ×10. (B) HMVEC-d cells were transfected with 1 μg of GFP-WT or GFP-K44A dynamin plasmid. After 24 h, cells were infected with KSHV at an MOI of 10 for different times and KSHV internalization was measured by real-time DNA PCR. Histogram shows internalized copy numbers of KSHV in HMVEC-d cells transfected with WT and K44A dynamin plasmids. (C and D) Dynasore did not affect internalization in HUVEC (C) and HMVEC-d (D) cells. HUVEC cells and HMVEC-d cells grown in six-well plates were treated with 80 μM dynasore for 1 h at 37°C and infected with KSHV at an MOI of 10 for different times, and KSHV internalization measured by real-time DNA PCR for ORF73 gene. (E) Dynasore treatment affects KSHV internalization in HFF cells. Cells grown in six-well plates were treated with 100 μM dynasore and infected with KSHV at an MOI of 10 for different times, and KSHV internalization measured by real-time DNA PCR. Histogram shows the internalized copy numbers of KSHV DNA with and without dynasore treatment. Each reaction was done in duplicate, and each bar represents the mean ± standard deviation of the results of three experiments.

pends upon the lipid raft and mitogen-activated protein kinase signaling pathway (22). Influenza virus enters cells predominantly via clathrin-mediated endocytosis and has been studied extensively as a model for clathrin-mediated endocytosis (52, 53). However, by combining inhibitory methods to block both clathrin-mediated endocytosis and uptake by caveolae in the same cell, it was demonstrated that influenza virus infects cells by an additional, nonclathrin-dependent, noncaveolar-dependent endocytic pathway (53). Our studies confirm our earlier findings that KSHV enters HFF cells by the clathrin pathway and suggest that KSHV entry varies according to the type of cells. The reason for this is not clear at present and could

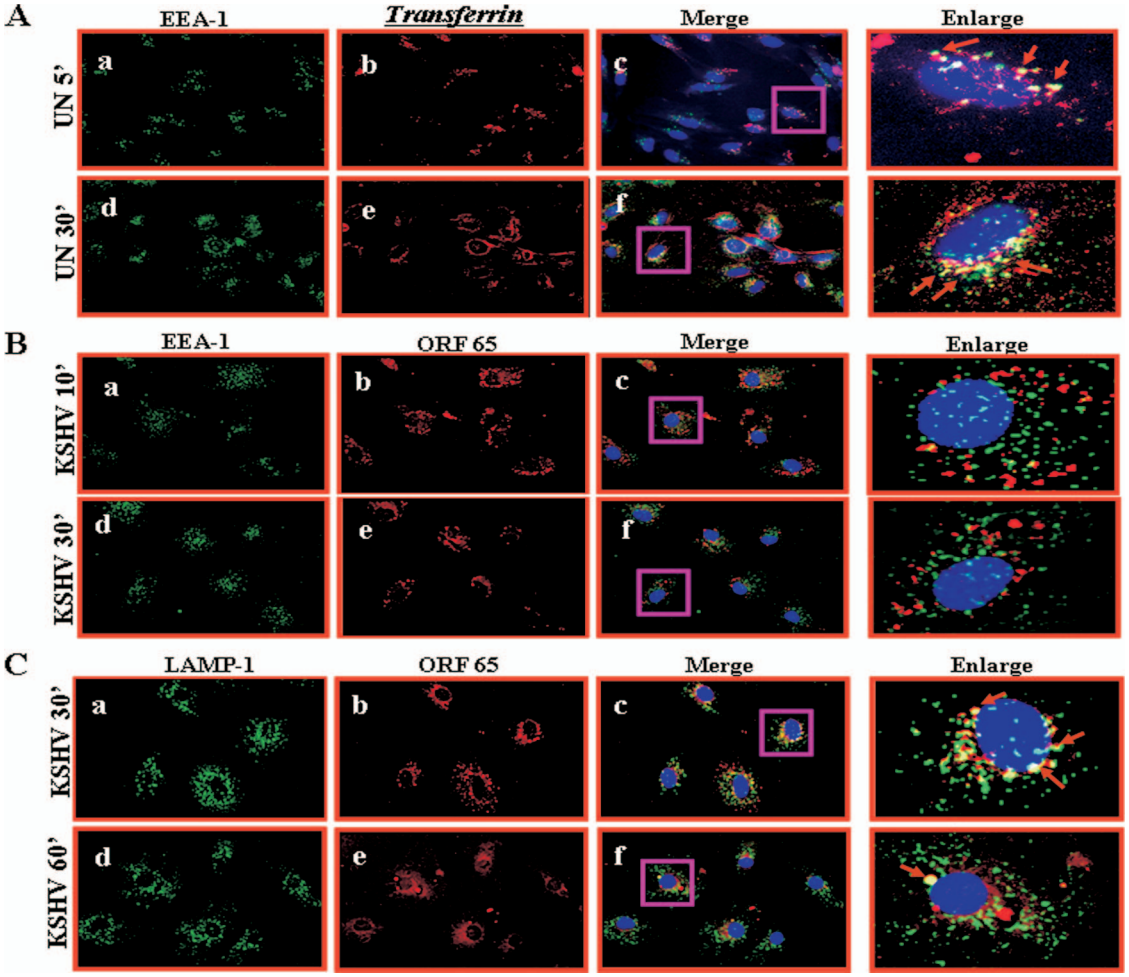

FIG. 8. KSHV trafficking in HMVEC-d cells and association with early and late endosomes. (A) Uptake of transferrin. Uninfected cells were pulsed with Alexa Fluor 594-tagged transferrin (25 μg/ml) for 5 min or 30 min at room temperature, fixed, permeabilized, washed in PBS, blocked with 5% BSA, and incubated with anti-mouse EEA-1 antibodies for 1 h at room temperature. The cells were washed, reacted with secondary antibodies, washed, mounted in antifade reagent with DAPI, and visualized under a fluorescence microscope. Red arrows indicate colocalization of transferrin with EEA-1. Magnification, ×40. (B and C) HMVEC-d cells grown in eight-chamber slides were infected with KSHV at an MOI of 10 for the indicated times, fixed, permeabilized, and stained with mouse anti-EEA-1 or anti-LAMP-1 and rabbit anti-ORF65 antibodies for 1 h at room temperature. Cells were washed, incubated with anti-mouse Alexa Fluor 488 (green) and anti-rabbit Alexa Fluor 594 (red) antibodies for 30 min at room temperature, washed, mounted in DAPI, and visualized. Red arrows indicate colocalization of KSHV capsid and LAMP-1. Magnification, ×40. Boxed areas are shown enlarged in the right-hand panels. ', min; UN, uninfected.

represent subtle differences in the density and nature of the receptor engaged and/or the type of accessory molecules and signal pathways engaged in the different types of cells. Similar results have been observed for entry of other viruses.

The kinetics of KSHV entry and nuclear delivery of viral DNA in HUVEC cells showed a trend similar to that observed in HMVEC-d cells (21). Similar to our observations, Yoo et al. (67) also demonstrated that infection of HUVEC cells results in the early and sustained expression of the latent transcripts; however, they also observed the expression of a cascade of immediate early, early, and late lytic gene expression starting from 16 h p.i. Our studies showed expression of the lytic cycle switch ORF50 expression as early as 2 h p.i., with peaking at 8 h p.i. and a subsequent decline. Since the percentage of cells expressing the lytic cycle genes was not examined by Yoo et al. (67), the observed lytic cycle gene cascade could represent a low percentage of cells entering into spontaneous lytic cycle replication.

Macropinocytosis appears to be an important mode of entry by many viruses. For example, vaccinia virus (27), adenovirus types 3 and 5 (26), foot and mouth disease virus (46), human immunodeficiency virus type 1 (22, 23), rubella virus in vero cells (19), and baculovirus in human hepatoma cells (25) have been shown to enter cells by macropinocytosis.

Macropinocytosis is associated with actin polymerization and membrane ruffling and has been shown to activate acid-dependent penetration from endosomes and the macropinosomal vesicles (26, 39). Macropinocytosis-induced macropinosomes are heterogeneous in size and are believed to be regulated at different stages. One of the important levels of regulation is the merger of the macropinosome with the endosomal pathway (18). It has been shown that macropinocytic

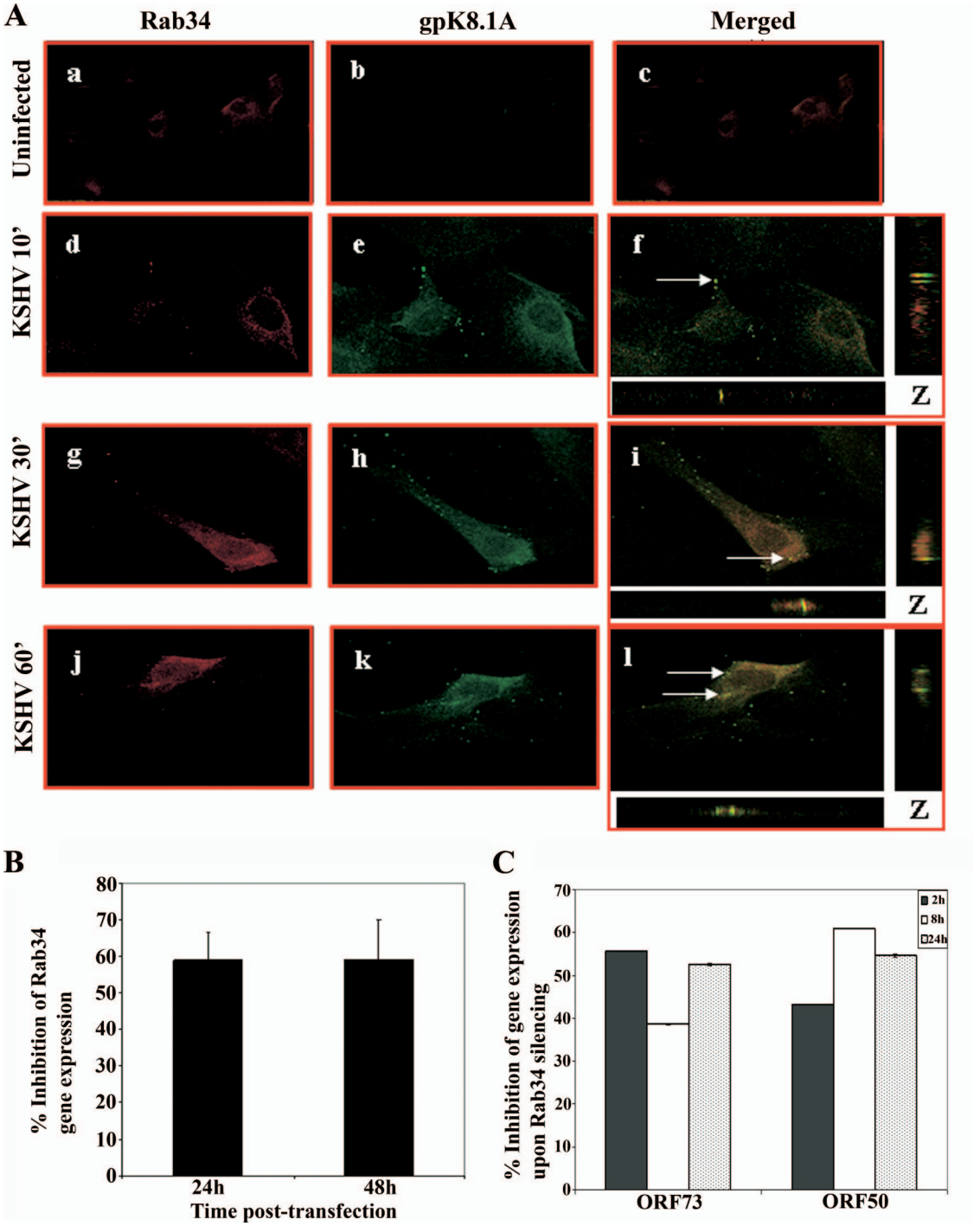

FIG. 9. KSHV trafficking in HMVEC-d cells and association with Rab34. (A) HMVEC-d cells grown in eight-chamber slides were infected with KSHV at an MOI of 10 for different times, washed, fixed in 4% paraformaldehyde, permeabilized, and stained with goat anti-Rab34 antibodies and with anti-gpK8.1A mAb for 1 h at room temperature. The cells were washed and incubated with anti-mouse Alexa Fluor 488 (green) and anti-rabbit Alexa 594 Fluor (red) antibodies, washed, mounted, and visualized with a confocal laser scanning microscope, and the data analyzed by using Olympus Fluoview software. Arrows indicate areas of colocalization of virion particles with Rab34. Magnification, ×40. ', min. (B) Histogram representing percent inhibition of Rab34 gene expression in HMVEC-d cells after 24 h and 48 h of transfection with si-Rab34 and si-C as described in Materials and Methods. Percent inhibition was calculated using Rab34 expression in si-C-transfected HMVEC-d cells as 100%. Each bar represents the average ± standard deviation of the results of three independent experiments. (C) Histogram representing the percent inhibition of ORF50 and ORF73 gene expression upon Rab34 silencing in HMVEC-d cells. The percent inhibition was calculated by considering levels of ORF50 or ORF73 in si-C-transfected cells infected with KSHV to be 100%. Each bar represents the average ± standard deviation of the results of three independent experiments.

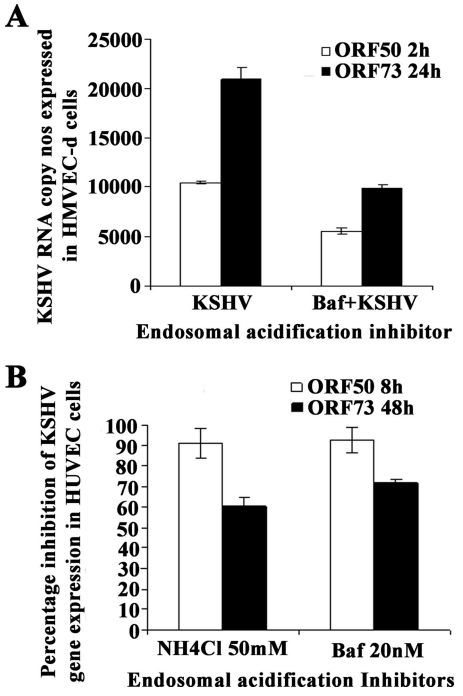

FIG. 10. KSHV requires a low-pH environment for infection. HMVEC-d (A) and HUVEC (B) cells were left untreated or pretreated with nontoxic concentrations of bafilomycin (Baf) or NH_4Cl for 1 h at 37°C, washed, and infected with KSHV at an MOI of 10 (10 DNA copies/cell), and total RNA isolated at the indicated time points. Fifty nanograms of DNase-treated RNA/μl was subjected to real-time RT-PCR as described in the Fig. 2A and 5D legends. Histograms depict the percent inhibition of KSHV ORF73 and ORF50 gene RNA copy numbers in the presence of indicated nontoxic concentrations of drugs, calculated in comparison to copy numbers in cells incubated with virus alone. Each reaction was done in duplicate, and each bar represents the mean ± standard deviation of the results of three independent experiments.

vesicles can become acidic and can intersect with the endocytic vesicles (16). EEA-1 association was not seen in KSHV infection of HMVEC-d cells, which is not surprising as EEA-1 has not been consistently associated with macropinosome formation (28, 41). We observed the colocalization of KSHV with LAMP-1, a marker for the late endosome. Sun et al. (58) have shown that Rab34 was associated with macropinosomes which colocalized with actin and also with large vesicles adjacent to the ruffles of fibroblast cells. The association of Rab34 with KSHV suggests that Rab34 could have a major role in KSHV infection, and our studies with siRNA clearly demonstrated its role in infection. Studies are in progress to further decipher the role of Rab34 GTPase in KSHV infection of endothelial cells.

Macropinocytosis is divided into a recycling and a processive type. Recycling macropinosomes are generated by the binding of growth factors, such as epidermal growth factor and nerve growth factor, to their respective receptors, which induces tyrosine kinases and is followed by activation of Rac1 and Cdc42 GTPases (15, 16, 35, 61). In the processive type of macropinocytosis, the macropinosomes shrink in size and mix with the late endosomes and lysosomes (42). Processive macropinocytosis is mediated by a diverse group of receptors, including integrins ($\alpha v\beta 3/\beta 5$ and $\alpha 5\beta 1$), mannose receptor, and lipopolysaccharide receptor CD14. Adenovirus 3 and 5 enter host cells by clathrin-mediated endocytosis involving dynamin (26). These viruses also enter into the same cells by macropinocytosis, which involves signaling through αV integrins, F-actin, Rho family GTPases, and protein kinase C but not dynamin. It is interesting to note that KSHV utilizes $\alpha v\beta 5$, $\alpha v\beta 3$, and $\alpha 3\beta 1$ integrins for entry into HMVEC-d cells and induces the host cells' preexisting signal pathways, such as focal adhesion kinase, Src, PI3-K, RhoA GTPases, extracellular signal-regulated kinases 1 and 2, and NF-kB, that are critical for entry and infection of cells (43, 47, 59). Further studies are in progress to determine the role of the various signaling molecules involved in macropinocytic entry.

Our earlier studies have shown that lipid raft disruption does not affect KSHV entry into HMVEC-d cells but affects transport of viral DNA toward the infected-cell nuclei due to reduced activation of PI3-K and RhoA GTPase signal molecules (43). Though macropinocytosis is used for entry in both types of endothelial cells, there were also some differences within the two endothelial cell types used. For example, lipid raft inhibitors blocked viral gene expression in HMVEC-d cells and not in HUVEC cells, thus suggesting that the association of the various signal molecules with lipid rafts may vary among endothelial cells; additional studies are required to evaluate their role in KSHV infection. Studies by Amstutz et al. (5) have shown that dynamin-independent macropinocytosis is an infectious entry route for human adenovirus type 3 in epithelial and hematopoietic cells. PAK1 is activated during adenovirus and vaccinia virus entry and is believed to play a role in macropinocytosis (5, 27). PAK1 associates with PI3-K during macropinocytosis (38). Since PI3-K is activated early during infection of endothelial cells by KSHV (43, 51), PAK1 activation by KSHV in endothelial cells could play a role in macropinocytic entry. Further evaluation of the role of PAK1 in KSHV infection of endothelial cells would shed more light on the infectious process of this important pathogen.

ACKNOWLEDGMENTS

This study was supported in part by Public Health Service grant AI 057349 and funding from the Rosalind Franklin University of Medicine and Science H. M. Bligh Cancer Research Fund to B.C.

We thank Mark A. McNiven, Department of Biochemistry and Molecular Biology and the Miles and Shirley Fiterman Center for Digestive Diseases, Mayo Clinic, Rochester, MN, for plasmids Dyn-WT and dyn-K44A. We thank Keith Philibert for critically reading the manuscript.

REFERENCES

1. **Akula, S. M., P. P. Naranatt, N.-S. Walia, F.-Z. Wang, B. Fegley, and B. Chandran.** 2003. Kaposi's sarcoma-associated herpesvirus (human herpesvirus 8) infection of human fibroblast cells occurs through endocytosis. J. Virol. **77:**7978–7990.
2. **Akula, S. M., N. P. Pramod, F. Z. Wang, and B. Chandran.** 2001. Human herpesvirus 8 envelope-associated glycoprotein B interacts with heparan sulfate-like moieties. Virology **284:**235–249.
3. **Akula, S. M., N. P. Pramod, F. Z. Wang, and B. Chandran.** 2002. Integrin alpha3beta1 (CD 49c/29) is a cellular receptor for Kaposi's sarcoma-associated herpesvirus (KSHV/HHV-8) entry into the target cells. Cell **108:**407–419.
4. **Akula, S. M., F. Z. Wang, J. Vieira, and B. Chandran.** 2001. Human herpesvirus 8 interaction with target cells involves heparan sulfate. Virology **282:**245–255.
5. **Amstutz, B., M. Gastaldelli, S. Kalin, N. Imelli, K. Boucke, E. Wandeler, J. Mercer, S. Hemmi, and U. F. Greber.** 2008. Subversion of CtBP1-controlled macropinocytosis by human adenovirus serotype 3. EMBO J. **27:**956–969.
6. **Antman, K., and Y. Chang.** 2000. Kaposi's sarcoma. N. Engl. J. Med. **342:**1027–1038.

7. **Bais, C., B. Santomasso, O. Coso, L. Arvanitakis, E. G. Raaka, J. S. Gutkind, A. S. Asch, E. Cesarman, M. C. Gershengorn, and E. A. Mesri.** 1998. G-protein-coupled receptor of Kaposi's sarcoma-associated herpesvirus is a viral oncogene and angiogenesis activator. Nature **391:**86–89.
8. **Bechtel, J. T., Y. Liang, J. Hvidding, and D. Ganem.** 2003. Host range of Kaposi's sarcoma-associated herpesvirus in cultured cells. J. Virol. **77:**6474–6481.
9. **Chang, Y., E. Cesarman, M. S. Pessin, F. Lee, J. Culpepper, D. M. Knowles, and P. S. Moore.** 1994. Identification of herpesvirus-like DNA sequences in AIDS-associated Kaposi's sarcoma. Science **266:**1865–1869.
10. **Dourmishev, L. A., A. L. Dourmishev, D. Palmeri, R. A. Schwartz, and D. M. Lukac.** 2003. Molecular genetics of Kaposi's sarcoma-associated herpesvirus (human herpesvirus 8) epidemiology and pathogenesis. Microbiol. Mol. Biol. Rev. **67:**175–212.
11. **Ganem, D.** 1998. Human herpesvirus 8 and its role in the genesis of Kaposi's sarcoma. Curr. Clin. Top. Infect. Dis. **18:**237–251.
12. **Ganem, D.** 1997. KSHV and Kaposi's sarcoma: the end of the beginning? Cell **91:**157–160.
13. **Gao, S. J., J. H. Deng, and F. C. Zhou.** 2003. Productive lytic replication of a recombinant Kaposi's sarcoma-associated herpesvirus in efficient primary infection of primary human endothelial cells. J. Virol. **77:**9738–9749.
14. **Grundhoff, A., and D. Ganem.** 2004. Inefficient establishment of KSHV latency suggests an additional role for continued lytic replication in Kaposi sarcoma pathogenesis. J. Clin. Investig. **113:**124–136.
15. **Hall, A.** 1998. Rho GTPases and the actin cytoskeleton. Science **279:**509–514.
16. **Hewlett, L. J., A. R. Prescott, and C. Watts.** 1994. The coated pit and macropinocytic pathways serve distinct endosome populations. J. Cell Biol. **124:**689–703.
17. **Hutt-Fletcher, L. M.** 2007. Epstein-Barr virus entry. J. Virol. **81:**7825–7832.
18. **Jones, A. T.** 2007. Macropinocytosis: searching for an endocytic identity and role in the uptake of cell penetrating peptides. J. Cell. Mol. Med. **11:**670–684.
19. **Kee, S. H., E. J. Cho, J. W. Song, K. S. Park, L. J. Baek, and K. J. Song.** 2004. Effects of endocytosis inhibitory drugs on rubella virus entry into VeroE6 cells. Microbiol. Immunol. **48:**823–829.
20. **Kieff, E., and A. B. Rickinson.** 2002. Epstein-Barr virus and its replication, p. 2511–2573. *In* D. M. Knipe and P. M. Howley (ed.), Fields virology. Lippincott, Wiliams & Wilkins, Philadelphia, PA.
21. **Krishnan, H. H., P. P. Naranatt, M. S. Smith, L. Zeng, C. Bloomer, and B. Chandran.** 2004. Concurrent expression of latent and a limited number of lytic genes with immune modulation and antiapoptotic function by Kaposi's sarcoma-associated herpesvirus early during infection of primary endothelial and fibroblast cells and subsequent decline of lytic gene expression. J. Virol. **78:**3601–3620.
22. **Liu, N. Q., A. S. Lossinsky, W. Popik, X. Li, C. Gujuluva, B. Kriederman, J. Roberts, T. Pushkarsky, M. Bukrinsky, M. Witte, M. Weinand, and M. Fiala.** 2002. Human immunodeficiency virus type 1 enters brain microvascular endothelia by macropinocytosis dependent on lipid rafts and the mitogen-activated protein kinase signaling pathway. J. Virol. **76:**6689–6700.
23. **Marechal, V., M. C. Prevost, C. Petit, E. Perret, J. M. Heard, and O. Schwartz.** 2001. Human immunodeficiency virus type 1 entry into macrophages mediated by macropinocytosis. J. Virol. **75:**11166–11177.
24. **Marsh, M., and A. Pelchen-Matthews.** 2000. Endocytosis in viral replication. Traffic **1:**525–532.
25. **Matilainen, H., J. Rinne, L. Gilbert, V. Marjomaki, H. Reunanen, and C. Oker-Blom.** 2005. Baculovirus entry into human hepatoma cells. J. Virol. **79:**15452–15459.
26. **Meier, O., K. Boucke, S. V. Hammer, S. Keller, R. P. Stidwill, S. Hemmi, and U. F. Greber.** 2002. Adenovirus triggers macropinocytosis and endosomal leakage together with its clathrin-mediated uptake. J. Cell Biol. **158:**1119–1131.
27. **Mercer, J., and A. Helenius.** 2008. Vaccinia virus uses macropinocytosis and apoptotic mimicry to enter host cells. Science **320:**531–535.
28. **Miaczynska, M., S. Christoforidis, A. Giner, A. Shevchenko, S. Uttenweiler-Joseph, B. Habermann, M. Wilm, R. G. Parton, and M. Zerial.** 2004. APPL proteins link Rab5 to nuclear signal transduction via an endosomal compartment. Cell **116:**445–456.
29. **Mocarski, E. S., Jr.** 1997. Propagating Kaposi's sarcoma-associated herpesvirus. N. Engl. J. Med. **336:**214–215.
30. **Naranatt, P. P., S. M. Akula, and B. Chandran.** 2002. Characterization of gamma2-human herpesvirus-8 glycoproteins gH and gL. Arch. Virol. **147:**1349–1370.
31. **Naranatt, P. P., S. M. Akula, C. A. Zien, H. H. Krishnan, and B. Chandran.** 2003. Kaposi's sarcoma-associated herpesvirus induces the phosphatidylinositol 3-kinase-PKC-ζ-MEK-ERK signaling pathway in target cells early during infection: implications for infectivity. J. Virol. **77:**1524–1539.
32. **Naranatt, P. P., H. H. Krishnan, M. S. Smith, and B. Chandran.** 2005. Kaposi's sarcoma-associated herpesvirus modulates microtubule dynamics via RhoA-GTP-diaphanous 2 signaling and utilizes the dynein motors to deliver its DNA to the nucleus. J. Virol. **79:**1191–1206.
33. **Nicola, A. V., A. M. McEvoy, and S. E. Straus.** 2003. Roles for endocytosis and low pH in herpes simplex virus entry into HeLa and Chinese hamster ovary cells. J. Virol. **77:**5324–5332.
34. **Nicola, A. V., and S. E. Straus.** 2004. Cellular and viral requirements for rapid endocytic entry of herpes simplex virus. J. Virol. **78:**7508–7517.
35. **Nobes, C., and M. Marsh.** 2000. Dendritic cells: new roles for Cdc42 and Rac in antigen uptake? Curr. Biol. **10:**R739–R741.
36. **Nobes, C. D., and A. Hall.** 1995. Rho, rac, and cdc42 GTPases regulate the assembly of multimolecular focal complexes associated with actin stress fibers, lamellipodia, and filopodia. Cell **81:**53–62.
37. **Pan, H., J. Xie, F. Ye, and S.-J. Gao.** 2006. Modulation of Kaposi's sarcoma-associated herpesvirus infection and replication by MEK/ERK, JNK, and p38 multiple mitogen-activated protein kinase pathways during primary infection. J. Virol. **80:**5371–5382.
38. **Papakonstanti, E. A., and C. Stournaras.** 2002. Association of PI-3 kinase with PAK1 leads to actin phosphorylation and cytoskeletal reorganization. Mol. Biol. Cell **13:**2946–2962.
39. **Pelkmans, L., and A. Helenius.** 2003. Insider information: what viruses tell us about endocytosis. Curr. Opin. Cell Biol. **15:**414–422.
40. **Pfeffer, S. R.** 2001. Rab GTPases: specifying and deciphering organelle identity and function. Trends Cell Biol. **11:**487–491.
41. **Porat-Shliom, N., Y. Kloog, and J. G. Donaldson.** 2008. A unique platform for H-Ras signaling involving clathrin-independent endocytosis. Mol. Biol. Cell **19:**765–775.
42. **Racoosin, E. L., and J. A. Swanson.** 1993. Macropinosome maturation and fusion with tubular lysosomes in macrophages. J. Cell Biol. **121:**1011–1020.
43. **Raghu, H., N. Sharma-Walia, M. V. Veettil, S. Sadagopan, A. Caballero, R. Sivakumar, L. Varga, V. Bottero, and B. Chandran.** 2007. Lipid rafts of primary endothelial cells are essential for Kaposi's sarcoma-associated herpesvirus/human herpesvirus 8-induced phosphatidylinositol 3-kinase and RhoA-GTPases critical for microtubule dynamics and nuclear delivery of viral DNA but dispensable for binding and entry. J. Virol. **81:**7941–7959.
44. **Rappocciolo, G., H. R. Hensler, M. Jais, T. A. Reinhart, A. Pegu, F. J. Jenkins, and C. R. Rinaldo.** 2008. Human herpesvirus 8 infects and replicates in primary cultures of activated B lymphocytes through DC-SIGN. J. Virol. **82:**4793–4806.
45. **Renne, R., D. Blackbourn, D. Whitby, J. Levy, and D. Ganem.** 1998. Limited transmission of Kaposi's sarcoma-associated herpesvirus in cultured cells. J. Virol. **72:**5182–5188.
46. **Rigden, R. C., C. P. Carrasco, A. Summerfield, and K. C. McCullough.** 2002. Macrophage phagocytosis of foot-and-mouth disease virus may create infectious carriers. Immunology **106:**537–548.
47. **Sadagopan, S., N. Sharma-Walia, M. V. Veettil, H. Raghu, R. Sivakumar, V. Bottero, and B. Chandran.** 2007. Kaposi's sarcoma-associated herpesvirus induces sustained NF-κB activation during de novo infection of primary human dermal microvascular endothelial cells that is essential for viral gene expression. J. Virol. **81:**3949–3968.
48. **Schnatwinkel, C., S. Christoforidis, M. R. Lindsay, S. Uttenweiler-Joseph, M. Wilm, R. G. Parton, and M. Zerial.** 2004. The Rab5 effector Rabankyrin-5 regulates and coordinates different endocytic mechanisms. PLoS Biol. **2:**E261.
49. **Schulz, T. F.** 1998. Kaposi's sarcoma-associated herpesvirus (human herpesvirus-8). J. Gen. Virol. **79**(Pt. 7)**:**1573–1591.
50. **Schulz, T. F., J. Sheldon, and J. Greensill.** 2002. Kaposi's sarcoma associated herpesvirus (KSHV) or human herpesvirus 8 (HHV8). Virus Res. **82:**115–126.
51. **Sharma-Walia, N., P. P. Naranatt, H. H. Krishnan, L. Zeng, and B. Chandran.** 2004. Kaposi's sarcoma-associated herpesvirus/human herpesvirus 8 envelope glycoprotein gB induces the integrin-dependent focal adhesion kinase-Src-phosphatidylinositol 3-kinase-rho GTPase signal pathways and cytoskeletal rearrangements. J. Virol. **78:**4207–4223.
52. **Sieczkarski, S. B., and G. R. Whittaker.** 2002. Dissecting virus entry via endocytosis. J. Gen. Virol. **83:**1535–1545.
53. **Sieczkarski, S. B., and G. R. Whittaker.** 2002. Influenza virus can enter and infect cells in the absence of clathrin-mediated endocytosis. J. Virol. **76:**10455–10464.
54. **Sinzger, C.** 2008. Entry route of HCMV into endothelial cells. J. Clin. Virol. **41:**174–179.
55. **Sivakumar, R., N. Sharma-Walia, H. Raghu, M. V. Veettil, S. Sadagopan, V. Bottero, L. Varga, R. Levine, and B. Chandran.** 2008. Kaposi's sarcoma-associated herpesvirus induces sustained levels of vascular endothelial growth factors A and C early during in vitro infection of human microvascular dermal endothelial cells: biological implications. J. Virol. **82:**1759–1776.
56. **Somsel Rodman, J., and A. Wandinger-Ness.** 2000. Rab GTPases coordinate endocytosis. J. Cell Sci. **113**(Pt. 2)**:**183–192.
57. **Staskus, K. A., W. Zhong, K. Gebhard, B. Herndier, H. Wang, R. Renne, J. Beneke, J. Pudney, D. J. Anderson, D. Ganem, and A. T. Haase.** 1997. Kaposi's sarcoma-associated herpesvirus gene expression in endothelial (spindle) tumor cells. J. Virol. **71:**715–719.
58. **Sun, P., H. Yamamoto, S. Suetsugu, H. Miki, T. Takenawa, and T. Endo.** 2003. Small GTPase Rah/Rab34 is associated with membrane ruffles and

macropinosomes and promotes macropinosome formation. J. Biol. Chem. **278:**4063–4071.

59. **Veettil, M. V., S. Sadagopan, N. Sharma-Walia, F.-Z. Wang, H. Raghu, L. Varga, and B. Chandran.** 2008. Kaposi's sarcoma-associated herpesvirus forms a multimolecular complex of integrins ($\alpha V\beta 5$, $\alpha V\beta 3$, and $\alpha 3\beta 1$) and CD98-xCT during Infection of Human Dermal Microvascular Endothelial Cells, and CD98-xCT is essential for the postentry stage of infection. J. Virol. **82:**12126–12144.
60. **Veettil, M. V., N. Sharma-Walia, S. Sadagopan, H. Raghu, R. Sivakumar, P. P. Naranatt, and B. Chandran.** 2006. RhoA-GTPase facilitates entry of Kaposi's sarcoma-associated herpesvirus into adherent target cells in a Src-dependent manner. J. Virol. **80:**11432–11446.
61. **Veithen, A., P. Cupers, P. Baudhuin, and P. J. Courtoy.** 1996. v-Src induces constitutive macropinocytosis in rat fibroblasts. J. Cell Sci. **109**(Pt. 8)**:**2005–2012.
62. **Vieira, J., P. O'Hearn, L. Kimball, B. Chandran, and L. Corey.** 2001. Activation of Kaposi's sarcoma-associated herpesvirus (human herpesvirus 8) lytic replication by human cytomegalovirus. J. Virol. **75:**1378–1386.
63. **Wang, D., Q. C. Yu, J. Schroer, E. Murphy, and T. Shenk.** 2007. Human cytomegalovirus uses two distinct pathways to enter retinal pigmented epithelial cells. Proc. Natl. Acad. Sci. USA **104:**20037–20042.
64. **Wang, F.-Z., S. M. Akula, N. P. Pramod, L. Zeng, and B. Chandran.** 2001. Human herpesvirus 8 envelope glycoprotein K8.1A interaction with the target cells involves heparan sulfate. J. Virol. **75:**7517–7527.
65. **Watanabe, T., M. Sugaya, A. M. Atkins, E. A. Aquilino, A. Yang, D. L. Borris, J. Brady, and A. Blauvelt.** 2003. Kaposi's sarcoma-associated herpesvirus latency-associated nuclear antigen prolongs the life span of primary human umbilical vein endothelial cells. J. Virol. **77:**6188–6196.
66. **Whittaker, G. R., and A. Helenius.** 1998. Nuclear import and export of viruses and virus genomes. Virology **246:**1–23.
67. **Yoo, S. M., F. C. Zhou, F. C. Ye, H. Y. Pan, and S. J. Gao.** 2005. Early and sustained expression of latent and host modulating genes in coordinated transcriptional program of KSHV productive primary infection of human primary endothelial cells. Virology **343:**47–64.
68. **Zhong, W., H. Wang, B. Herndier, and D. Ganem.** 1996. Restricted expression of Kaposi sarcoma-associated herpesvirus (human herpesvirus 8) genes in Kaposi sarcoma. Proc. Natl. Acad. Sci. USA **93:**6641–6646.